Redistribution of riverine and rainfall freshwater by the Bay of Bengal circulation

Akurathi Venkata Sai Chaitanya, Jérôme Vialard, Matthieu Lengaigne, Francesco d'Ovidio, Jean Riotte, Fabrice Papa, Rathinam Arthur James

Ocean Dynamics
2021, Volume 71, Pages 1113-1139
https://doi.org/10.1007/s10236-021-01486-5
https://archimer.ifremer.fr/doc/00724/83616/

Redistribution of riverine and rainfall freshwater by the Bay of Bengal circulation

Chaitanya Akurathi Venkata Sai [1, *], Vialard Jérôme [2], Lengaigne Matthieu [3], D'ovidio Francesco [2], Riotte Jean [4], Papa Fabrice [5], James Rathinam Arthur [1]

[1] Department of Marine Science, Bharathidasan University, Tiruchirappalli, India
[2] LOCEAN-IPSL, Sorbonne Université (UPMC, Univ Paris 06)-CNRS-IRD-MNHN, Paris, France
[3] MARBEC, University of Montpellier, CNRS, IFREMER, IRD, Sète, France
[4] GET, CNRS-IRD-UPS-CNES, Toulouse, France
[5] LEGOS, Université de Toulouse, IRD/CNRS, CNES/UPS, Toulouse, France

* Corresponding author : Akurathi Venkata Sai Chaitanya, email address : chaitu.ocean1@gmail.com

Abstract :

We use satellite-derived currents and a Lagrangian approach to investigate the redistribution of the precipitation minus evaporation (P-E) and river freshwater inputs into Bay of Bengal (BoB) by the oceanic circulation. We find a key role of Ekman transport in shaping the BoB freshwater distribution. Until September, the summer monsoon winds induce eastward Ekman transport, which maintains freshwater near its major rivers and rain sources in the northeastern BoB. The winter monsoon Ekman transport strongly contributes to the surface flow in many areas of the interior BoB. This ~ 0.15 m s−1 westward transport overcomes the weaker offshore transport by mesoscale motions and pushes a ~ 40/45% mixture of P-E and Ganges–Brahmaputra freshwater into the East Indian Coastal Current (EICC). In agreement with previous studies, we find that the EICC then transports Ganges–Brahmaputra freshwater southward, allowing the formation of a narrow freshwater tongue or "river in the sea" along the coast east of India in November. Ekman transport thus operates jointly with the EICC to allow the "river in the sea" formation. The EICC is nonetheless a "leaky pipe" as only ~ 22% of the Ganges–Brahmaputra, and ~ 9% of the P-E monsoonal freshwater inputs exit the BoB near Sri Lanka. The winter monsoon anticyclonic circulation in fact brings more rain freshwater from the equatorial Indian Ocean into the southeastern BoB than it exports freshwater through the EICC. As a result, the BoB circulation contributes to a net freshwater gain that amounts to 11% of the local rain and freshwater inputs.

Keywords : Freshwater, Bay of Bengal, Oceanic circulation, Satellite altimetry, Mesoscale eddies, Ekman transport, Lagrangian approach

1. Introduction

The Bay of Bengal (hereafter, BoB, black frame on Figure 1a) is under the influence of the Indian summer monsoon. As a result, it is a dilution basin, which annually receives more freshwater by rain (~6400 km^3) and rivers (~3020 km^3) than it loses some through evaporation (~4150 km^3; Figure 1c). This large freshwater input into a relatively small, semi-enclosed basin yields low near-surface salinity and contributes to marked surface haline stratification during and after the monsoon (Shetye et al. 1991; 1996; Vinayachandran et al. 2002; Behara and Vinayachandran, 2016; Sengupta et al. 2016). This strong salinity stratification has important implications, because it inhibits vertical mixing (e.g. de Boyer et al. 2007; Thadathil et al. 2016; Krishnamohan et al. 2019). Salinity stratification indeed reduces the cooling under tropical cyclones in the BoB right after the monsoon (Sengupta et al. 2008; Neetu et al. 2012), allowing a stronger surface evaporation that sustains the cyclone intensification (Neetu et al. 2019). The BoB haline stratification also inhibits the upward mixing of nutrients, and probably contributes to the low biological productivity in the BoB (Prasanna Kumar et al. 2002; Sarma et al. 2016). These impacts of the BoB haline stratification are thus a strong incentive to study its hydrological cycle and the controls of its salinity distribution.

The BoB receives its largest freshwater supply from May to December, due to the rainfall and river inputs during the southwest monsoon (June to September) period (Figure 1c). Most southwest monsoon rainfall occurs in the northeastern BoB (Figure 1a), where there are also several major river systems, with maximum runoffs during and shortly after the southwest monsoon (Figure 1c, Fekete et al. 2002; Dai and Trenberth, 2002; Papa et al. 2012). These riverine freshwater inputs are dominated by the Ganges-Brahmaputra-Hooghly system at the northern head of the BoB (Figure 1d; hereafter GB, 47% of the annual river freshwater input) and Irrawaddy-Salween river system in the northeastern BoB (IRS, 29 %, see Figure 1a for location). After October, there is a shift to the winter monsoon, and most excess precipitation occurs in the southern BoB (Figure 1b).

The BoB is a semi-enclosed basin, and the excess freshwater it receives has to be approximately balanced by export through its southern boundary at annual and longer timescales (Vinayachandran et al. 2013). Circulation also plays a critical role for redistributing freshwater within the BoB (e.g. Rao et al. 2011; Sengupta et al. 2016; Sree Lekha et al. 2018; Akhil et al.

2014; Behara and Vinayachandran, 2016) and creates strong horizontal salinity gradients during and after the monsoon (Gordon et al. 2016; Wijesekera et al. 2016).

The BoB geometry and monsoon annual cycle induce a complete reversal of surface currents with a cyclonic circulation during winter and an anti-cyclonic one during summer (Schott and McCreary, 2001; Shankar al., 2002). The BoB interior circulation is closed to the west by the East Indian Coastal Current (EICC), a narrow, coastally-trapped flow along the east coast of India. The EICC flows northward before and during the summer monsoon, but reverses to form a southward current from October onward (see Figure 2c; Shetye et al. 1996; Sherin et al. 2018). The EICC is not only driven by local winds. Wind stress curl in the BoB interior can indeed influence the EICC through Rossby waves propagation, while upstream wind variations along the equator or other parts of the Bay can propagate as equatorial and then coastal Kelvin waves to the east coast of India (McCreary et al. 1996; Shankar et al. 1996). Despite some remote wind contribution from other BoB regions and the equatorial band, the southward EICC flow during the northeast monsoon is largely caused by local alongshore wind stress and offshore Ekman pumping (McCreary et al. 1996).

In this paper, we are mostly focusing on the EICC effect on the freshwater distribution, not on the EICC dynamics itself. The large freshwater flux from rain and rivers induces an intense northern BoB freshening during and shortly after the summer monsoon (see Figure 2ab; Shetye et al. 1991; Han et al. 2001; Rao and Sivakumar, 2003; Sengupta et al. 2006; Akhil et al. 2014, Pant et al. 2015). The post-monsoon EICC transports part of this freshwater southward, creating a narrow, ~100 to 200km wide "river in the sea" along the east coast of India after September (see Figure 2c; Shetye et al. 1996; Chaitanya et al. 2014; Akhil et al. 2014). By November, this freshwater plume usually extends all the way down to Sri Lanka (Fournier et al. 2017a; Akhil et al. 2020). There, the westward-flowing Northeast Monsoon Current export its freshwater toward the southeastern Arabian Sea (e.g. Jensen, 2001; Durand et al. 2007), where it is thought to influence surface temperature and the monsoon onset (e.g. Durand et al. 2004; Masson et al. 2005; Vinayachandran et al. 2007). Observational evidence however suggests that this export is quite intermittent (Hormann et al. 2019). While the southward expansion of this "river in the sea" along the east coast of India can largely be attributed to advection, its decay, from December onwards (Figure 2d), largely results from the upward mixing of deeper, saltier water (Akhil et al. 2014).

In addition to this seasonal signal, the BoB circulation is strongly modulated at intraseasonal timescales by mesoscale eddies, especially in the western BoB where the strong horizontal shear of the EICC yields high eddy kinetic energy levels (Chelton et al. 2011; Chen et al. 2018). This strong eddy activity yields discontinuous meandering flow patterns along the EICC (Durand et al. 2009; Sherin et al. 2018). The strong salinity gradient between the fresh coastal regions in the northern and western BoB and the saltier interior is energetically stirred by the intense mesoscale activity, that exports freshwater to the BoB interior while bringing offshore saltier water to the coast along the "river in the sea" (Hareeshkumar et al. 2013, Fournier et al. 2017a; Sree Lekha et al. 2018; Mahadevan et al. 2016; Benshila et al. 2014). Analyses of moored measurements similarly indicate that horizontal advection dominates the Sea Surface Salinity (SSS) evolution at intraseasonal timescales in the BoB interior (Rao et al. 2011; Sengupta et al. 2016; Sree Lekha et al. 2018).

One interesting question is how can freshwater remain in the coastally-trapped EICC and be advected southward to form the "river in the sea" if the offshore export by eddies is so strong? We hypothesize that the northeastward transport by Ekman currents during the southeast monsoon can offset the effect of eddies, and push and maintain freshwater into the EICC. Some observational studies indeed suggest a strong effect of Ekman transport on the freshwater distribution. For instance, Vinayachandran et al. (2002) found that the southwestward Ekman transport during the southwest monsoon advected surface freshwater past their mooring site in the central northern BoB. Closer to the east coast of India, Gopalakrishna et al. (2002) found that the offshore Ekman transport maintained freshwater away from the coast during the southwest monsoon. While these two observational studies point towards a strong impact of the Ekman transport on the freshwater distribution locally, they mostly concern the southwest monsoon and there has been to our knowledge no study trying to systematically assess its importance at the basin-scale. That will be one of the objectives in this manuscript.

The current paper aims at investigating the details of the freshwater redistribution by the BoB horizontal circulation. More precisely, we want to address the following questions: How does the circulation affect the distribution of post-monsoon freshwater contributions from rivers and P-E? What are the respective roles of the various components of the circulation (e.g. geostrophic vs. Ekman, large scale circulation vs. mesoscale eddies etc…) in redistributing the freshwater? How much does the surface circulation contribute to the export of freshwater at the BoB southern

boundary? In particular, how can such a well-defined "river in the sea" form along the east coast of India given the strong offshore export by meso-scale eddies? We have chosen to adopt a Lagrangian approach based on satellite-derived geostrophic and Ekman surface currents to track the fate of the freshwater inputs to BoB. Such method was used to track freshwater from rivers before, for instance by Fournier et al. (2017b) to study interannual variations in the offshore spreading of the Amazon-Orinoco river freshwater plumes into the tropical Atlantic Ocean. To our knowledge, the only other study that used such an approach applied to the freshwater transport in the BoB is Mahadevan et al. (2016). That study concluded that sub-mesoscale processes and vertical mixing induced a strong saltening of the "river in the sea" water parcels along their southward path, in agreement with the modelling results of Akhil et al. (2014). As we will see, the main original results from our study is identifying the importance of Ekman transport for the BoB freshwater distribution, and showing that the BoB circulation brings more freshwater into the Andaman Sea to the southwest than it exports freshwater through the EICC to the southeast.

This paper is organized as follows. Section 2 describes the datasets and methodology that we use to decompose the oceanic circulation into its various components. It also introduces and validates the Lagrangian tool that we use. Section 3 illustrates how the Lagrangian method is used to separately track freshwater associated with surface precipitation and riverine inputs, and qualitatively illustrates the effect of Ekman transport and mesoscale eddies. Section 4 then introduces a quantitative mapping of the contribution of various sources to the BoB freshening. It also presents box-averaged freshwater budgets for the entire BoB, and key regions such as the east coast of India where the "river in the sea" forms. Finally, section 5 summarizes and discusses our results, including a comparison with other studies and the key limitations of our approach.

2. Data and Methodology

2.1. Data sets and gridded surface current validation

Below, we describe the surface currents dataset that is used as input of our Lagrangian method, the datasets that we use to estimate the BoB freshwater budget (precipitation, evaporation, river runoffs), as well as ancillary validation datasets. All the products below are used over the 2000-2016 period, except the SMOS satellite SSS dataset (2010-2016).

The net freshwater flux at the ocean surface is obtained from the Precipitation minus Evaporation budget. Evaporation is obtained from the daily latent heat fluxes at the ocean surface in the TropFlux dataset (Praveen Kumar et al. 2012). For precipitation, we use the three-hourly, 0.25° resolution merged multi-satellite and rain gauges Tropical Rainfall Measuring Mission (TRMM) 3B42 precipitation product (Huffman et al. 2007). We also use the Global Precipitation Climatology Project (GPCP) dataset (Adler et al. 2003) in the discussion section of this paper, to evaluate the sensitivity of our results to the precipitation dataset.

This study includes all the major rivers feeding the BoB (Figure 1b for locations), namely: the Ganges-Brahmaputra-Hoogly (hereafter, GB), the Irrawady-Salween (hereafter, IRS), the Mahanadi-Brahmani, Godavari and Krishna on the east coast of India, and several other rivers on the Northeastern BoB rim (most notably the Kaladan, hereafter MGKNE). The GB (47%) and IRS (29%) account for 76% of the total climatological river freshwater into the BoB (Figure 1d; numbers based on Fekete et al. 2002). The MGKNE account for 10% of the annual BoB riverine inputs. The remaining 13% are accounted for by a multitude of much smaller rivers, that we neglect in the current study. Overall, when also including rainfall and evaporation, we account for 92-94% the BoB net freshwater balance (Table 1). In section 5, we will discuss the impacts of missing rivers and uncertainties in the river runoff estimates based on estimates from Decharme et al. (2019).

We use direct estimates of the GB and IRS interannually-varying runoffs estimated from altimetry by Papa et al. (2012) and India Water Resource Information System (http://indiawrisgov.in/) interannual runoffs for M and GK. These values were tuned to match Fekete et al. (2002) climatological values, with a scaling factor to account for the Salween and Hooghly (not accounted for in Papa et al. 2012). We used Fekete et al. (2002) climatological values for the Kaladan river system (NE).

We use the version-3 gridded Soil Moisture and Ocean Salinity (SMOS) satellite SSS data (Boutin et al. 2018) over 2010-2016 to compute the BoB climatological SSS. Akhil et al. (2020) indeed show that this product compares well with in situ observations and other satellite products over the BoB.

We use the Geostrophic and Ekman Current Observatory (GEKCO) surface current dataset (Sudre et al. 2013), which provides daily estimates of geostrophic and Ekman currents on a $1/4^0$ grid, representative of the weekly average centred on that day. The geostrophic currents are derived

from the SSALTO/DUACS (Segment Sol Multi-missions d'Altimétrie, d'Orbitographie et de Localisation Précise/Multi-mission Altimeter Data Processing System) sea level dataset (Dibarboure et al. 2011) with support from CNES. The Ekman currents are derived using wind data from the SeaWinds microwave scatterometer onboard the QuikSCAT (Sudre et al. 2013 for more details).

Our study strongly relies on the GEKCO surface currents product, and it is hence important to assess its realism, in particular near the coast. For that, we use velocities deduced from finite differences of satellite-tracked Surface Velocity Program (SVP) drifting buoys (Lumpkin et al. 2016). SVP positions are quality-controlled and archived at AOML (Atlantic Oceanographic and Meteorological Laboratory) Drifting Buoy Data Assembly centre. Figure 3 provides comparison of BoB surface currents estimates from GEKCO with those of all co-located drifters over 2000-2016 (a total of 120 individual drifters, representing ~150 000 velocity estimates). The GEKCO currents have 0.62 correlation with SVP currents, and mean absolute error of 0.13 $m.s^{-1}$. They tend to underestimate the in-situ currents (regression coefficient of 0.77). There is however no systematic bias in the direction estimate, and with most SVP directions within 45° of the satellite currents (MAE of 40° when retaining only currents above 0.2 $m.s^{-1}$ to avoid direction indetermination at low velocities). While these errors may appear large, one must remember that we compare punctual, instantaneous measurements with satellite estimates representative of 25 km x 25 km x 1 week blocks. Near-inertial oscillations are for example not resolved by the satellite measurements, while they always represent a large component of the near surface variations in the real ocean. The bottom line is that, despite these relatively large errors due to unresolved phenomena in the large-scale satellite dataset, the GEKCO dataset provides a reasonable, although smoother, representation of the BoB circulation. This will be further illustrated by comparison between GEKCO-based Lagrangian trajectories and real drifter trajectories in the following section.

2.2. The Lagrangian advection method and its validation

The Lagrangian advection package used here is that described in d'Ovidio et al. (2009) and Lehahn et al. (2018). It computes the trajectory of a hypothetical, passively-advected particle using the GEKCO surface currents product described in section 2.1. The daily, ¼° resolution velocity fields are linearly interpolated in time and space to provide the velocity at the particle position,

which is updated using a 3-hour time step. In order to avoid grounding of particle, we prescribe a 1 $m.s^{-1}$ oceanward velocity along the coast, which in practice "throws back" stranded particles into the ocean. We have checked that the results are insensitive to this specific choice of oceanward velocities. We model unresolved currents by the satellite product (spatial scales below about 70 km, i.e. small mesoscale eddies and sub-mesoscale motions) by adding a random noise to the currents, as described in pp. 224-225 of Cotté et al. (2011). The amplitude of this random noise is set to correspond to a lateral mixing coefficient of 300 $m^2.s^{-1}$. This value is chosen as it matches that typically used in ¼° resolution numerical models (e.g. Akhil et al. 2014), the same resolution as our surface currents product.

In order to illustrate the performance of the Lagrangian scheme, Figure 3cd shows the comparison of two real SVP drifter trajectories and an ensemble of 30-day long Lagrangian trajectories (corresponding to 6 different realizations of the random noise forcing described above) re-initialized every 10-day along the drifter path. Since Durand et al. (2009) expressed doubts about the capacity altimeter-derived gridded currents to resolve the EICC, we selected two drifter trajectories that sample the southward-flowing EICC after the monsoon. Figure 3cd shows that the simulated Lagrangian trajectories follow the path of the actual drifters remarkably well. This suggests that our strategy is able to reproduce actual surface particle trajectories, even in the narrow, coastally trapped EICC reasonably well, and that we can rely on this method to understand the freshwater pathways within the BoB.

2.3. Surface circulation decomposition

One of our objectives is to identify the roles of various components of the surface circulation (e.g. Ekman vs. geostrophic; large-scale vs. mesoscale eddies) on the freshwater fate. To do so, we separate the circulation into those components. The GEKCO product conveniently provides the geostrophic and Ekman components of the surface circulation: Figure 2abcd show the full surface currents, while Figure 2efgh only shows the Ekman component. The GEKCO estimate of the geostrophic and Ekman components qualitatively matches those displayed in previous (e.g. Shankar et al. 2002) and recent (Raj 2017) studies. We compare control experiments that include the full currents (described in section 2.4) with experiments that only retain the geostrophic component, in order to evaluate the effect of the Ekman transport.

We further want to separate the effect of mesoscale eddies from those of the large-scale circulation in spreading the BoB freshwater. To that end, we decompose the daily total surface circulation into its large-scale and small-scale components. The most obvious large-scale current component is the daily seasonal cycle, simply obtained as the 2000-2016 seasonal average. But there is also a large-scale modulation of this current system by the Indian Ocean Dipole (IOD; e.g. Rao et al. 2002, Aparna et al. 2012; Akhil et al. 2016; Sherin et al. 2018), a mode of climate variability anchored in the equatorial Indian Ocean (Saji et al. 1999; Webster et al. 1999) that peaks in boreal fall (September to November). We isolate large-scale current signals associated with the IOD through an Empirical Orthogonal Function (EOF) statistical analysis of sea-level interannual anomalies in the BoB, as previously done by Suresh et al. (2018). The two leading EOFs represent 28% of the total variance (note that the results in this paper do not change if only the leading EOF is used), and efficiently represent signals associated with the IOD. The residual from the seasonal cycle and two leading EOFs is defined as the eddy field.

Figure 4 displays an example of the sea-level and surface currents decomposition for November 2006, a positive IOD year. At that time of the year, the climatological EICC flows southward along the entire East Indian coast (Figure 4b). The large-scale interannual current anomalies during a positive IOD year are anticyclonic (Figure 4c), corresponding to a weakening of the EICC, in good agreement with the results in Suresh et al. (2018) and Akhil et al. (2016). The residual is shown in Figure 4d, and mostly corresponds to smaller, mesoscale structures. This example indicates that our simple decomposition strategy method successfully separates large-scale signals associated with the seasonal cycle and IOD anomalies from mesoscale features. The decomposition also works well for other dates (not shown). The standard deviation of each component of the flow (second row in Figure 4) clearly indicates that eddies contribute most to the total kinetic energy. Furthermore, the eddy distribution closely corresponds to that discussed in e.g. Chelton et al. (2011) or Chen et al. (2018), with strongest eddy variability in the western BoB (Figure 4d), another indication that our simple decomposition method performs relatively well at decomposing the flow into large-scale (seasonal+IOD) and synoptic currents features mostly associated with mesoscale eddies.

2.4. Lagrangian experiments

We use Lagrangian trajectories computed using the d'Ovidio et al. (2009) and Lehahn et al. (2018) package to advect freshwater inputs from various sources (rivers, net precipitation minus evaporation) forward in time. Simulations are run for each year over the 2000-2016 period, and we display 2000-2016 averages. These simulations can be run with the full GEKCO currents ("CTL" experiment in table 2), or based on geostrophic ("no-Ekman" or NOEK) or large-scale ("no-eddies" or NOED) surface currents, as defined in section 2.3. The NOEK (NOED) minus CTL differences allow to evaluate the effect of Ekman currents (mesoscale variability).

In section 3, we will first illustrate the effect of the circulation *qualitatively* by showing the evolution of particles initially released in the main source regions (figures 5 and 6). We will describe the more comprehensive set of experiments and method used to obtain *quantitative* freshwater distribution associated with each source in section 4.1, and will discuss these *quantitative* estimates in the rest of section 4.

3. Qualitative overview of the freshwater redistribution by the surface circulation

The objective of this section is not to separate the rainfall and river contributions (this will be done in section 4), but just to *qualitatively* illustrate the effect of the total circulation (subsection 3.1), and of the Ekman transport and eddies (subsection 3.2) on virtual particles released in high freshwater input regions, that are mostly located in the northeastern BoB. These two subsections will be illustrated from the 15th September and December distributions of particles released on the 15th of August (at the peak of freshwater inputs to the BoB, Figure 1c). The 15th September maps will illustrate the effects of the summer monsoon circulation (Figure 2ab) on the freshwater distribution, and the 15th December maps that of the winter monsoon circulation (Figure 2c).

3.1. Transport by the BoB circulation

In July and September (summer monsoon), the circulation is predominantly eastward (Figure 2ab). The surface freshening is still mostly concentrated in the vicinity of the river mouths, with SSS values as low as 20 pss there (Figure 2b). A cyclonic circulation develops throughout the BoB in November (winter monsoon), with most intense currents along the entire Indian coast in the southward-flowing EICC (Figure 2c). Associated with this, there is a northwestward shift of the IRS freshwater plume, and an expansion of the GB plume along the east coast of India (Figure 2c).

By January, the EICC has almost entirely disappeared, and the winter monsoon westward Ekman drift strongly contributes to the surface circulation (Figure 2dh).

Figure 5bc illustrates the September and December 15th distributions of particles released on the 15th of August (Figure 5a) near the GB, IRS and MGKNE river mouths, and the average currents since the particles release. Particles released near the GB river mouth have mostly spread southwestward by September, but remain confined north of 16°N due to the main circulation pattern (Figure 5e). This is understandable along the coast, where the EICC flows southward, but occurs against the mean circulation in some regions: we will see that this is mainly due to eddies in section 3.2. The full development of the southward EICC from September to December yields a very clear expansion of particles originating from the GB river mouth along the coast of India, as far south as Sri Lanka by December. This supports the idea that advection is the main driver of the seasonal development of a "river in the sea" after the monsoon along the coast of India (Shetye et al. 1996; Jensen, 2001; Chaitanya et al. 2014; Akhil et al. 2014; Fournier et al. 2017a; Akhil et al. 2020).

Particles released near the IRS river mouth expand less than those released near the GB mouth, in particular due to the weaker large-scale circulation on the eastern than on the western boundary of the BoB. The highest density of particles released near the IRS however starts expanding ~300-400 km westward from September to December, qualitatively reflecting the observed SSS evolution (Figure 2). We will see in section 3.2 that this can be attributed to the effect of Ekman transport.

Figure 5def illustrates the evolution of the density of particles that were initially uniformly distributed in the northeastern BoB, the region of highest freshwater input through precipitation minus evaporation during the monsoon. This will allow a first qualitative overview of how the horizontal circulation spreads this freshwater. Since this region intersects that of the GB and IRS boxes, there are of course common features with them. First, particles expand in a narrow band along the coast of India under the influence of the post-summer monsoon southward flowing EICC (Figure 5ef), as those from GB (Figure 5c). Second, there is a clear northwestward shift of particles located in the broad IRS region between September and December (Figure 5bc). One can finally notice some limited southward expansion of the edge of the initial particle distribution against the mean currents in some regions, as did happen near the GB river mouth. Again, we will show in the next section that this is due to eddies.

3.2. Effect of Ekman drift and meso-scale Eddies

The left column of Figure 6 displays the September and December 15th density of particles initially released in the northeastern BoB box on August 15th for the CTL experiment again (i.e. same as Figure 5d). This column can be compared to the right column, from the NOED experiment described in section 2.4 to get a feel for the effect of eddies on the freshwater transport. Particles initially released at the river mouths locations of Figure 5a illustrate the same qualitative features (not shown).

Mesoscale eddies are often represented as lateral Laplacian diffusion in low-resolution models. Their potential role in carrying freshwater across large salinity gradients has also been highlighted specifically in the BoB (e.g. Hareeshkumar et al. 2013, Fournier et al. 2017a; Benshila et al. 2014). Comparing left and right columns on Figure 6 confirms that eddies contribute to spreading freshwater horizontally. Particles in the EICC are indeed more confined to the coast in the NOED than in the CTL experiments (compare Figure 6c with 6d). Mesoscale motions thus tend to export freshwater from the post-monsoon "river in the sea" along the coast of India toward the BoB interior, as already noted in the above-cited studies. Mesoscale motions also explain why freshwater sometimes seems to expand against the mean currents, as noted in section 3.1: while particles are confined northward of 12°N in December in NOED (Figure 6c), they expand as far south as 8°N in the Andaman sea in the CTL experiment (Figure 6d), despite a circulation that is on average northward (Figure 5f).

The Ekman transport is veered 90° right relative to the mean wind direction in the northern hemisphere, and is hence predominantly southeastward during the summer monsoon (Figure 2ef) and northwestward during the winter monsoon (Figure 2gh). By September, there is thus an overall ~4° (almost 500 km) eastward shift of the particles distribution due to Ekman transport during the summer monsoon (Figures 6a and 7a). The overall effect of Ekman transport during the summer monsoon is thus to "push" freshwater eastward, to the Myanmar coast and into the Andaman Sea. This is very clear in Figure 7b, which shows the CTL minus NOEK particles density distribution: at the end of the summer monsoon, the Ekman transport has contributed to increase the quantity of freshwater in the northern Andaman Sea and along the coast of Myanmar, and to decrease it in the central northern BoB. The situation is very different in December, two months after the onset of the northeast monsoon and westward Ekman transport (Figures 6c and 7c). In the northeastern

BoB, the westward Ekman transport removes freshwater from the IRS outlet region, and pushes it northwestward into the Northern BoB (Fig. 7d). Further south, the highest concentration of GB particles hugs the coast of India much more in the CTL than in the NOEK experiment (Figures 6c and 7c). This indicates that, during the winter monsoon, the shoreward Ekman transport helps pushing freshwater into the coastally-trapped, southward flowing EICC, increasing the freshwater quantity at the coast and diminishing it offshore (Figure 7d).

Red vectors on Figure 2e-h indicate locations where the climatological zonal Ekman current is more than 2/3 of the total zonal current. Ekman currents tend to be weaker than geostrophic currents in regions of intense currents such as the EICC or in the Sri Lanka Dome region. On the other hand, Ekman currents are very homogenous over the basin, systematically pushing the freshwater eastward at 0.15 $m.s^{-1}$ (the BoB average climatological zonal Ekman current in august in GEKCO) during the summer monsoon, and westward at 0.1 $m.s^{-1}$ (average in November) during the winter monsoon. Red vectors on Figure 2e-h indicate that Ekman currents end up being an important contributor to the total zonal climatological flow over large portions of the BoB interior. A simple back-of-the envelope computation with the above numbers show that Ekman currents alone would result in a ~1000 km systematic eastward or westward displacement during the typical 3-month duration of each monsoon. This effect will of course combine with that of geostrophic currents and eddies, but it will help systematically pushing freshwater southwestward until October and northeastward until December or January. Overall, the winter monsoon Ekman transport overcomes the effect of eddies on the post-monsoon "river in the sea": while eddies tend to export freshwater offshore, the Ekman transport tend to "push back" the freshest water toward the coast (we will demonstrate this more quantitatively in section 4). Finally, the Ekman transport during the winter monsoon also contributes to the northwestward expansion of the IRS plume (not shown), as discussed in the previous section.

4. Freshwater transport by the surface circulation

Up to this point, we have just *qualitatively* illustrated the pathways of freshwater into the BoB, and the effect of Ekman transport and eddies on these pathways. Below, we will first explain our experimental setup and methodology to obtain *quantitative* estimates of the freshwater thickness distributions from individual sources (section 4.1). We will then discuss the relative

contributions of these sources (section 4.2), and examine the freshwater budget for key BoB regions (including the whole BoB and east coast of India) in section 4.3.

4.1. From Lagrangian trajectories to a quantitative estimate of freshwater distribution

Let us describe our methodology for providing freshwater *quantitative* estimates separately for each source. Our method provides an estimate of the total quantity of freshwater (from either rain or rivers) that was brought at a given location by surface currents. In order to distinguish it from the usual definition of freshwater thickness (how much freshwater would be needed to explain the differences between a salinity profile and a reference profile, see e.g. Sengupta et al. 2006), we will hereafter designate this quantity as "Lagrangian freshwater thickness".

Most of the freshwater input over the BoB occurs during the May to September period (Figure 1). We have thus run forward Lagrangian integrations for virtual particles released on the 15th of June, July, August, September, October, November and December. Particles are released every 0.025° over the entire northern Indian Ocean (40-120°E, north of 10°S). Releasing particles everywhere in the northern Indian Ocean allows to track the transport of freshwater inputs corresponding to rain, including inputs from outside the BoB.

Each virtual particle tracks the amount of freshwater received in its vicinity (i.e. in a 0.025°x0.025° bin) during the preceding month. For each particle, we define 4 variables that separately keep track of the volume of freshwater respectively associated with rain, and the 3 river systems: GB (Ganges-Brahmaputra), IRS (Irrawady-Salween), and MGKNE (Mahanadi, Godavari, Krishna and other rivers on the coast of Myanmar). For all particles, the rain freshwater volume variable is set to the integral of P-E (precipitation minus evaporation) over the month preceding the particle release and surrounding 0.025° x 0.025° grid cell. We assume that particles located outside of the river mouths regions defined on Figure 5a were not influenced by rivers (their GB, IRS and MGKNE volumes are set to zero). If one particle is released in the vicinity of the GB (north of 19.5°N; blue on Figure 5a), IRS (93.5°E-98°E, 15°N-17°N; red on Figure 5a) or MGKNE (green on Figure 5a), we set the corresponding river freshwater volume to the integral of the river runoff over the preceding month divided by the number of particles within that box. Particles are then advected forward using satellite estimates of the total surface currents. As they are advected they do not acquire, or lose, any further freshwater. In order to obtain the Lagrangian freshwater thickness distribution, we sum freshwater volumes of all the particles in ½° x ½° bins,

and then divide by the bin area to obtain a thickness. This allows to get the Lagrangian freshwater thickness distribution associated to each source at any time.

The sketch of Figure 8 explains how the results of Lagrangian experiments initialized at various dates are combined to provide an estimate of the freshwater distribution, for the example of October. The October freshwater distribution is for instance obtained as the sum of the June (after 4 months of forward-advection), July (after 3 months), August (after two months) and September (after one month) freshwater inputs. Freshwater distributions are computed from the 15th of June to the 15th of December every year, and we display the 2000-2016 average. Differences between the control experiment (full currents) and sensitivity experiments with the geostrophic or large-scale currents (Table 2) allow to estimate contributions from the Ekman transport and meso-scale eddies, respectively. A 3 x 3 pixel bin spatial smoothing is then applied on maps for display purposes, but the raw fields are used in the budget computations of section 4.3.

4.2. Rain and rivers contributions to the freshwater distribution

Figure 9 shows the Lagrangian freshwater distributions associated with the GB, IRS and MGKNE runoffs on September and December 15th. These cumulated distributions reflect most of the features already discussed from Figures 5, 6 and 7. The GB freshwater input expands progressively along the Indian coast in the EICC, reaching ~16°N by September 15th and Sri Lanka by December 15th (Figure 9ad). The GB freshening signal along the northeast Indian coast by September 15th is consistent with observational findings of Shetye et al. (1991), who reported a freshwater plume (2 to 3pss fresher than the surrounding waters) that moves equatorward against local winds north of 16°N in August 1989. This study also reported a salinity increase near the coast, which they attributed to local upwelling. This observation is compatible with our discussion of the effect of the Ekman transport that maintains the freshwater away from the coast at this time (see Figure 6ab). The IRS freshwater input remains confined near the river mouths in September (Figure 9b), because Ekman transport maintains it close to the coast during the summer monsoon, where the large-scale circulation is weak (Figure 2bf). The IRS freshwater expands northwestward by December (Figure 9e), under the influence of the opposite Ekman flow during the winter monsoon (Figure 2cg). For readability, we multiplied freshwater inputs from other smaller rivers by three on Figure 9c,f. Rivers in the northeastern BoB have the same fate than the IRS (maintained near the coast by the eastward Ekman transport during the summer monsoon, and pushed westward

during the winter monsoon). Freshwater sources on the east coast of India have a comparable evolution to GB waters, and including Godavari-Krishna at 16°N: they are pushed eastward by the Ekman transport during the summer monsoon, and maintained in the southward-flowing EICC during the winter monsoon, allowing them to reach as far south as Sri Lanka.

Figure 10a shows the cumulated precipitation minus evaporation (i.e. net downward freshwater flux at the ocean surface) between the beginning of the monsoon (defined as May 15th) and September 15th (panel a) or December 15th (panel d). Both panels confirm that most of the surface freshwater input to the BoB occurs in the northeastern part of the basin (with more freshwater inputs in the southern part of the basin when including the winter monsoon months). These freshwater input maps can be compared to the corresponding Lagrangian freshwater thickness distributions (Figure 10be) to evaluate how the integrated effect of circulation redistributes freshwater horizontally. Figure 10cf displays the net effect of freshwater transport (i.e. whether advection locally adds or remove freshwater), obtained as maps of Lagrangian P-E freshwater thickness (b,e) minus the local P-E input (a,d). In September, the main effect of the summer monsoon circulation is to remove rainfall inputs from the western and central northern BoB, and "push" them against the BoB northeastern rim (Figure 10abc): i.e. the summer monsoon circulation concentrates rainfall in the regions of largest freshwater inputs. To the contrary, the winter monsoon circulation strongly redistributes rainfall from the regions of large inputs in the northeastern BoB (Figure 10d) to the BoB western rim (Figure 10ef). As detailed in the next paragraph, the Ekman transport plays an essential role in this freshwater redistribution.

Figure 11ad shows the September and December 15th total Lagrangian freshwater thickness distributions, including both contributions from rivers (Figure 9) and rainfall (Figure 10). In September, most of the freshwater is still relatively close to the sources (Figure 11a), with maxima near the GB and IRS river mouths, in the northeastern BoB and along the east coast of India, north of 16°N. There are two main noticeable changes between September and December: freshwater is no longer concentrated near sources but has invaded most of the northern BoB and the "river in the sea" has expanded southward along the east coast of India (Figure 11d). Figure 11 also illustrates the essential Ekman transport contribution to this freshwater redistribution, by comparing this distribution in the control experiment to that in the NOEK experiment (Figure 11b,e) and displaying their difference (Figure 11c,f). This confirms the essential role of Ekman transport for concentrating freshwater in the high freshwater input region to the northeastern BoB

during the summer monsoon (Figure 11a,b,c). Ekman transport is also largely responsible for shifting freshwater west during the winter monsoon, freshening the central northern BoB and allowing the EICC to export freshwater southward (Figure 11d,e,f). The "river in the sea" is indeed much more visible in December in the experiment with than without the Ekman transport (Fig 11d,e). The budget analysis of Figure 15 will qualitatively confirm the strong role of the Ekman transport in the existence and timing of the coastally-trapped freshening.

Figure 12 shows the September and December 15th contributions (in %) of individual freshwater sources (GB, IRS, P-E and MGKNE) to the total Lagrangian freshwater thickness distribution displayed on Figure 11a,d. P-E tends to always dominate the freshwater distribution (> 80%) in the southern (south of 16°N) and interior BoB (Figure 12cg). Rivers tend to have large contributions close to their mouth, as expected. The IRS locally contributes to up to 50% the freshening. This effect is concentrated in the northeastern Andaman Sea during the summer monsoon, and then expands westward into the central BoB during the winter monsoon, due to Ekman transport. In September, the Godavari and Krishna are the only freshwater inputs in the southwestern BoB and dominate the freshwater distribution there (Figure 12d, although the absolute freshwater quantity remains weak there, see Figure 11a), but they are completely overwhelmed by much larger freshwater inputs from the north during the winter monsoon (Figure 12h). The GB and P-E contributions indeed expands southward along the east coast of India (Figure 12e,g), due to the combined effect of the westward Ekman drift and southward advection in the EICC. Interestingly, rainfall and GB freshwater contribute roughly equally to the freshening along the east coast of India (Figure 12e,g). This is because the EICC entry point is both located near the GB river mouth (Figure 2b,c) and in a region of high rainfall (Figure 10a).

4.3. Regional budgets

To get a more quantitative insight on the effect of circulation in different regions, we now provide Lagrangian freshwater thickness budgets in various BoB regions, highlighted as blue boxes on Figure 11a. The total freshwater evolution H in each box is decomposed into the forced part H_f (simply the contribution of P-E, GB or, MGKNE or IRS inside each box) and the effect of transport by the circulation H_t (obtained as $H_t = H_l - H_f$ as on 9ure 8cf, where H_l is the total Lagrangian freshwater thickness obtained as described in section 4.1). This decomposition can be made separately for individual river sources and P-E, and the sensitivity experiments in Table 2

further allow splitting the transport contribution in large-scale currents vs. eddies, or in geostrophic currents vs. Ekman transport (e.g. the Ekman transport term is obtained as the transport in the CTL experiment minus that in the NOEK experiment).

At the scale of the entire BoB, local freshwater inputs strongly dominate the budget (Figure 13a) with P-E, GB, IRS and MGKNE respectively representing 53, 25, 16 % and 6% of the total BoB freshwater content by December. The effect of transport is comparatively small. The surface circulation only exports about 22% of the GB freshwater input outside of the BoB through the EICC by December (red and dashed curves in Figure 13a), *i.e.* most of the GB freshwater (and all of the IRS and MGKNE freshwater) recirculates horizontally within the BoB. Similarly, the transport contribution to the BoB P-E freshwater thickness is relatively small (about 11% of the May to December BoB freshwater input) and represents a net P-E gain for the BoB. I.e. overall, the circulation brings more surface freshwater inside the BoB than it exports freshwater from the BoB. This is puzzling, because a lot of studies have previously focussed on the freshwater *export* from the BoB in the EICC (e.g. Jensen 2001): where does the extra rain freshwater enter the BoB? The Lagrangian approach allows us to break this P-E freshening (11% of the May to December BoB local P-E input) into contributions from freshwater entering (green curve on Figure 13b) and exiting (yellow curve on Figure 13b) the BoB, and to show the initial and final distributions of these freshwater inputs / outputs (Figure 13c,e and 13d,f, respectively). As expected, the dominant exit route is associated with freshwater export to the southeastern Arabian Sea through the EICC (Figure 13f), as previously described (e.g. Jensen 2001; Durand et al. 2007). This net freshwater loss for the BoB only amounts to 16% of the local freshwater inputs by rain and rivers (Figure 13b). In this regard the EICC is not very efficient at transferring freshwater from the high input region in the northeastern BoB to the BoB "exit" near Sri Lanka. The horizontal circulation in facts brings more freshwater (Figure 13c, ~27% of the BoB P-E), than there is freshwater exiting through the EICC route. The Lagrangian approach indicates that the P-E freshwater input is mostly associated with rain that fell in the eastern equatorial Indian Ocean, to the southeast of the BoB (Figure 13c), which is a high rainfall region during the winter monsoon (Figure 1a). The BoB winter cyclonic circulation (Fig. 2cd) brings some of this rainfall into the Andaman sea (Figure 13e). Figure 13c indicates that there is also a weaker (not shown) contribution of rain that falls in the Southeastern Arabian Sea during the southwest monsoon (Figure 1a), through the North Monsoon Current. Overall, the original result from Figure 13 is that the BoB horizontal circulation

is associated with a net freshwater gain (11% of the total local rainfall), because there is more rain freshwater entering the southeastern BoB (27% of the total local rainfall) than leaving the BoB through the EICC route (16% of the total).

In the IRS region, river runoffs contribute to freshening about twice as much as local P-E (Figure 14a). The circulation first tends to bring P-E from outside the IRS box, due to the eastward Ekman drift during the southwest monsoon, before this tendency reverses and ends up exporting P-E (Figure 14a), due to the northwestward Ekman transport during the winter monsoon. Circulation on the other hand always exports IRS freshwater from the vicinity of the river mouth (about 71% of the IRS input by December). The rate of exported freshwater however increases during the winter monsoon, due to the offshore Ekman drift.

In the central BoB (Figure 14b), P-E dominates the freshening, both due to local rainfall (26% by December) and to its redistribution by the circulation (50% by December). The horizontal circulation indeed shifts rainfall from the high input region near Myanmar to the central northern BoB during the winter monsoon, mostly due to Ekman pumping (Figures 10d-f and 11d-f). The horizontal circulation comparatively brings much less river freshwater (with GB, IRS and MGKNE respectively contributing to 8%, 15% and 3% of the total freshening by December). The IRS water is largely brought to the BoB interior by the northwestward Ekman drift during the winter monsoon, as is the case for P-E.

In the vicinity of the GB river mouth, the GB is of course the main freshwater source, but P-E should not be underestimated, as it accounts for about 1/3 of the total local June-December freshwater input (Figure 14c). The horizontal circulation only adds very small P-E and IRS freshwater in the northern BoB box, but exports ~64% of the GB and ~79% of the MGKNE freshwaters by December (M and NE are both in the same region as the GB river mouth, see Figure 1a). As we have seen before, this export is largely associated with the southward transport by the EICC along the Indian coast (Figure 9df). The total contribution of advected P-E freshwater to the northern BoB box is relatively small, because P-E enters from the south due to the cyclonic circulation and northward component of the Ekman transport during winter, but then exits through the EICC (not shown). I.e. the northern BoB region exports a mixture of GB and rain freshwater southward into the western BoB (WBoB) box, defined as a strip along the east coast of India (Figure 11a).

This WBoB box has received a lot of attention before, because of the "river in the sea" that forms after the monsoon along the coast of India. We hence provide on Figure 15 a more detailed budget in this region. For this analysis, the M and NE rivers have been grouped to the GB because of their geographical proximity (red curves), and the Godavari and Krishna on the east coast of India are displayed separately (green curves). Our results show that the "river in the sea" is not only caused by the GB freshwater, but by a blend of GB (~44% by December) and P-E (~39%) freshwater brought by the EICC (Figure 15a). The freshening in the WBoB has only a small contribution from local rainfall input (about 6% by December) and IRS water brought by the EICC (about 4%). Rivers on the Indian peninsula provide non-negligible inputs to the WBoB box, but these inputs are almost entirely exported by the horizontal circulation (green curves on Figure 15a): we will see why below. Figure 15d shows the initial distribution of the P-E freshwater that contributes to the December WBoB freshening. This can be seen as the "watershed" of the WBoB where ocean variable currents replace the fixed topography in this traditional hydrological concept. Most of the rain that contributes to the "river in the sea" originates from the northern BoB, and is first transported northward toward the GB mouth by the winter monsoon circulation (Figure 2d,h), before being advected into the WBoB by the EICC.

Figure 15bc refines the WBoB budget by providing the contributions of transport by large-scale currents vs. eddies and geostrophic vs. Ekman currents for the two main contributors in this region (P-E, GB and GK). Previous studies have insisted on the fact that eddies export freshwater from the WBoB region (e.g. Hareeshkumar et al. 2013, Fournier et al. 2017a; 2016; Benshila et al. 2014). We also find that eddies contribute to freshwater loss from the WBoB (Figure 15b). The eddy-induced freshwater loss is relatively small for P-E and GB (less than 15 % by December), but plays an essential role for exporting local GK river freshwater offshore (Figure 15b), probably because the GK river mouth is located close to the most energetic eddy activity region in the BoB (Figure 4h). But overall, Ekman transport has a much larger effect (Figure 15c). Up to September, the Ekman transport in the offshore direction associated with the southwest monsoon almost cancels the GB and P-E freshwater input from the north by the geostrophic EICC (Figure 15c). I.e. freshwater that enters the EICC from the north almost immediately exits it eastward, due to the eastward Ekman current component during the summer monsoon. Similarly, local freshwater inputs from the GK rivers are high during the monsoon (Figure 1d), but largely exported offshore by the Ekman pumping (Figure 15c) that teams up with eddies (Figure 15b). The net result is that

the WBoB freshwater content does not increase much until September (Figure 15a), i.e. the eastward Ekman transport prevents the river in the sea formation before September, by exporting any EICC freshwater input offshore. After October, the wind reversal induces an onshore transport, and the WBoB freshwater content increases due to the Ekman transport contribution (black and red "dotted" curves on Figure 15c). On the other hand, the geostrophic currents (black and red "crossed" curves on Figure 15c) tend to induce a reduction of the WBoB freshwater content: this is due to the effect of eddies, but also to the fact that the freshwater inputs from the GB and rain in the northern BoB have decreased (Figure 1b,c).

Figure 15c thus quantitatively demonstrates that the Ekman transport plays a strong role in the "river in the sea" development. During the southwest monsoon, the eastward component of the Ekman transport makes it difficult for the water parcels from the GB or under the high P-E region in the northeastern BoB to reach the EICC "entrance" (see the WBoB "watershed" on Figure 15d), hence limiting the "river in the sea" development. During the winter monsoon, Ekman transport "pushes" the rain and river freshwater towards the coast, against the weaker effect of mesoscale eddies, and allows it to be efficiently transported southward by the coastally trapped EICC. In the absence of Ekman transport, the EICC would transport much less freshwater southward, resulting in a much less marked "river in the sea" (Figure 11d,e,f).

5. Summary and Discussion

5.1. Summary

In this paper, we use a Lagrangian method to estimate how the Bay of Bengal (BoB) horizontal monsoon circulation redistributes the large freshwater input from precipitation minus evaporation (P-E) and rivers (GB: Ganges-Brahmaputra-Hooghly; IRS: Irrawaddy-Salween; and MGKNE: Mahanadi-Godavari-Krishna and other rivers in the Northeast, notably the Kaladan) during and after the southwest monsoon. The Lagrangian method temporally integrates surface current estimates obtained from satellite data, which include both the geostrophic and Ekman components (GEKCO product, Sudre et al. 2013). Comparisons with velocity estimates from BoB drifter data over the 2000-2016 period indicate that this product provides an unbiased estimates of the current direction, but tends to underestimate in situ velocities by ~20%. The Lagrangian method

is however able to reasonably reproduce drifter trajectories, including in the coastally-trapped East Indian Coastal Current (EICC). The Lagrangian trajectories can be combined with observational estimates of P-E, GB, IRS and MGKNE to provide quantitative estimates of the freshwater redistribution from these individual sources by the circulation, including the part that can be attributed to either mesoscale eddies or Ekman transport.

The BoB (north of 6°N) receives most of its freshwater during May-December. P-E represents about 50% of the freshwater input during this period (Table 1). P-E dominates the freshwater budget in the southern BoB, away from coasts. Figure 16 provides a summary sketch on how horizontal circulation in the BoB redistribute monsoonal freshwater inputs at the end and after the summer monsoon. The Ekman current is an important contributor to the zonal flow in many areas of the BoB interior (Figure 2e-h), and clearly contributes to shape the BoB freshwater distribution. The IRS freshwater is maintained near the coast by Ekman transport during the southwest monsoon (Figure 16a), and its influence remains local, due to the relatively weak large-scale circulation in the eastern BoB. It expands northwestward in November and December, due to Ekman transport during the winter monsoon (Figure 16b). The GB and rainfall waters are also initially maintained in the northeastern BoB during the summer monsoon (Figure 16a), but are then shifted westward to the central northern BoB and east coast of India during the winter monsoon (Figure 16b). This plays a key role in the development of the "river in the sea" freshwater tongue along the east coast of India, by controlling freshwater inputs into the southward-flowing post-monsoon EICC. P-E and GB in fact contribute in roughly equal proportions to this "river in the sea", which drains both GB and high rainfall rates in the head of the Bay into the EICC entry gate near the GB river mouth. Towards the end of the southwest monsoon, the eastward Ekman transport first limits the freshwater inputs from GB and P-E into the EICC (Figure 17a). This is consistent with previous observations (e.g. Vinayachandran et al. 2002; Gopalakrishna et al. 2002). By October, the P-E and GB freshwater inputs into the northern BoB have almost come to a stop. Yet, the EICC has fully developed by November, and the shoreward Ekman transport associated with the winter monsoon overcomes the much weaker freshwater offshore export by mesoscale eddies (Figure 16b). This pushes a ~40%/45% mix of P-E and GB freshwater from the central BoB into the narrow, coastally trapped EICC, allowing it to transport freshwater along the coast all the way down to Sri Lanka (Figure 16b).

Our results indicate that only 22% of the GB and 9% of the P-E from May to December total freshwater inputs are exported outside the BoB through the EICC route in December, i.e. that the EICC is not very efficient at transporting the strong rain and GB freshwater inputs in the northern BoB southward along the Indian coast. This is largely because eastward Ekman transport during the southwest monsoon prevents water parcels from the high freshwater input regions in the northeastern BoB to efficiently access the EICC "entrance" (Figure 16a). The EICC only becomes efficient at transporting freshwater southward after October, when the wind and Ekman transport have reversed (Figure 16b), but when freshwater inputs to the northern BoB have become much smaller. In fact, the BoB horizontal circulation is associated with a net freshwater gain. This is because eastern equatorial Indian Ocean rain brought into the southeastern BoB during the southwest monsoon overcomes freshwater losses through the EICC, resulting in a net BoB freshwater gain of ~11% of the local ~5200 to 5800 km^3 inputs through evaporation minus precipitation and rivers.

5.2. Discussion

Previous studies did already highlight the role of advection by the EICC for the "river in the sea" development along the coast of India after the monsoon (e.g. Shetye et al. 1996; Chaitanya et al. 2014; Akhil et al. 2014; Fournier et al. 2017a; Akhil et al. 2020), and the role of mesoscale eddies in the offshore salinity export from the "river in the sea" (Hareeshkumar et al. 2013; Benshila et al. 2014; Fournier et al. 2017a; Sree Lekha et al. 2018; Mahadevan et al. 2016). Our results confirm these findings. Our two main original results are the importance of Ekman transport for the BoB freshwater distribution, and the identification of a BoB net freshwater gain, associated with the northward transport of heavy rain from the equatorial Indian Ocean. As far as we know, the strong influence of the Ekman transport on the BoB freshwater distribution has been much less discussed than that of, e.g., the EICC. While Shetye et al. (1996) observations of the "river in the sea" in December 1991 do not specifically discuss the role of Ekman transport in maintaining the freshwater near the coast, the wind field they describe and downward sloping of isohalines they observe at the coast are consistent with it. The results of the idealized ocean model experiments of Sandeep and Pant (2019) are also consistent with our results on the role of the Ekman transport on the trapping of the "river in the sea" freshwater into the EICC. While not explicitly discussing the effects of Ekman transport, Sandeep and Pant (2019) indeed evaluate the impact of an idealized

wind forcing on the freshwater distribution, and find that freshwater remains along the coast under northeasterlies but is exported towards the central BoB under southwesterlies. Freshwater inputs into the southeastern BoB have also, as far as we know, not been discussed before, with most authors concentrating on freshwater exports by the EICC in the clearly visible "river in the sea" (e.g. Jensen 2001). While the "river in the sea" is important because of its impact on the southeastern Arabian Sea freshwater budget and temperature evolution (see Durand et al. 2007 for a review), we find that its freshwater export is weaker than the freshwater inputs to the Andaman Sea associated with the winter monsoon cyclonic circulation. As a result, the BoB circulation contributes to a net freshwater gain that amounts to 11% of the local rain and freshwater inputs.

Our study also provides estimates of the relative contributions of rain and rivers to the BoB freshening, which tend to disagree between past studies. Our findings agree with those of Benshila et al. (2014), which used passive tracer experiments embedded in a regional high-resolution (1/12°) ocean model to investigate the rainfall and rivers freshwater spreading in the BoB. Although they use a different experimental strategy, based on modelling, their results also indicate that oceanic rainfall and GB freshwater equally contribute to the west coast of India post-monsoon freshening, and that IRS waters remain trapped in the northern half of the Andaman basin, due to the more sluggish circulation in this region. In line with other modelling studies (Akhil et al. 2014, 2016; Wilson and Riser, 2016), they also point out that vertical exchanges between the upper and deeper layers play a key role in restoring the freshwater plume to pre-monsoon saltier SSS. Our results on the other hand seem to contradict other modelling studies, which argue that runoff dominates northern and western BoB freshening, with a weaker contribution from rainfall (Behara and Vinayachandran, 2016; Sandeep et al. 2018). Let us now discuss if that can be explained by uncertainties in the freshwater inputs or the neglected rivers. The rivers we have included account for 92-94% of the BoB net freshwater inputs, depending on the rainfall product we consider (Table 1 obtained from Fekete et al. (2002) data, but Decharme et al. (2019) data yields similar values). The remaining rivers are mostly small and scattered round the BoB. In addition, the main rivers that we included to the south of the Indian peninsula (GK) only weakly contribute to the "river in the sea" freshening, because the offshore Ekman transport during the southwest monsoon (when their runoff is strongest) aided by vigorous eddies in this region (Figure 4h) exports most of the local river inputs offshore (Figure 15bc). We thus feel that it is unlikely that the neglected rivers strongly impact our results.

There are also uncertainties in the various freshwater input products in this study. For instance, we used the TRMM rainfall dataset that yields larger rainfall over the BoB (Figure 17a) than the GPCP dataset (Huffman et al. 1997). Our runoff estimates for the GB+IRS+MGKNE (constrained to match the Fekete et al. (2002) climatological data) on the other hand provide a larger freshwater input from rivers than the Decharme et al. (2019) independent dataset (Figure 17a). We can thus provide a lower bound to the P-E contribution to the freshwater distribution by using GPCP (the weaker of the two P-E freshwater input estimates) and Fekete et al. (2002) (the strongest of the two runoff freshwater input estimates), as done on Figure 17b. A close comparison with Figure 12g indicates slightly weaker P-E contributions to the freshening close to the GB and IRS river mouths, but an otherwise very similar contribution of rainfall, a ~ 40/45% mix of P-E and river water in the "river in the sea". This is an indication that our results are quite robust, despite forcing freshwater datasets uncertainties.

Our estimate of the effect of eddies on the freshwater transport probably has a large error bar. The current generation of current reconstruction from nadir altimeters only resolve geostrophic currents at spatial scales down to about 70 km, and hence miss the effect of sub-mesoscale motions and of the smallest eddies (especially in the northern Bay where the first Rossby radius of deformation is less than 70 km, Chelton et al. 1998). These fine spatial scales are thought to contribute to the salinity lateral mixing in the BoB (e.g. Mahadevan et al. 2016). In our study, they are crudely parameterized as an extra random noise on the currents in the Lagrangian trajectory computation, set to correspond to a lateral mixing coefficient of 300 $m^2.s^{-1}$. Future swath altimetry missions (Morrow et al. 2019) will allow a better description of currents at fine spatial scales and of their impact on the BoB salinity field horizontal stirring.

Our results emphasize a stronger role of the Ekman transport on the BoB freshwater distribution. This result of course depends on the ability of the GEKCO product to reproduce the Ekman component of currents. Statistics of comparison with drifters are degraded when the Ekman component of currents is neglected (not shown). Similarly, the current direction mean absolute error remains very weak when the statistics are computed separately for the summer and winter monsoons (not shown), during which the Ekman transport has opposite directions. Those two analyses, and the fact that the GEKCO current dataset has no direction bias relative to surface drifters estimate (Figure 1b) suggest that the Ekman surface currents in GEKCO are reasonable.

We however emphasize the need to estimate Ekman currents in the BoB more precisely from observations, given their strong influence on the freshwater and surface salinity distribution.

One of the big advantages of our study is that we use a current field deduced from observations to evaluate the freshwater redistribution by the circulation. One obvious shortcoming to our approach is however that we do not account for vertical mixing, which has been reported to act as non-negligible freshwater sink for the BoB mixed layer (e.g. Akhil et al. 2014, 2016; Wilson and Riser, 2016). In a sequel to the current study, we will use a passive tracer approach in a high resolution model of the BoB, that will trace freshwater inputs from individual rivers and rainfall into the BoB (i.e. a quantitative extension of the Benshila et al. (2014) qualitative study). This should allow better evaluating the effects of vertical mixing.

Acknowledgements

AVS Chaitanya's PhD was supported by an IRD (Institut de Recherche pour le Développement) "ARTS" Ph.D. grant. He thanks CSIR-NIO (National Institute of Oceanography), Goa, India and LOCEAN, Paris, France for hosting him during his Ph. D. He also thanks Dr. V.V.Gopalakrishna for his scientific support. GEKCO current data is provided by Joel Sudre from CNRS/LEGOS, Toulouse upon request (http://www.legos.obs-mip.fr/members/sudre/gekco_form). All other data that is used in the paper is accessible on web repositories (SVP-drifter: https://www.aoml.noaa.gov/phod/gdp/; TropFlux: https://incois.gov.in/tropflux/data_access.jsp; TRMM: http://disc.sci.gsfc.nasa.gov/precipitation; Fekete-river discharge: http://www.grdc.sr.unh.edu/html/Data/index.html) . M. Lengaigne thanks IRD for supporting a long stay at the CSIR-NIO in Goa, India. J. Vialard thanks CSIR-NIO for granting him an "Adjunct Scientist" position for a period of three years. This research was supported under the SARAL/AltiKa project, funded by CNES (Centre National d'Études Spatiales). The Lagrangian code we used is included in the SPASSO software package, which is freely available here: https://people.mio.osupytheas.fr/~doglioli/spasso.htm

References

Adler RF, G J Huffman, A Chang, R Ferraro, P Xie, J Janowiak, B Rudolf, U Schneider, S Curtis, D Bolvin, A Gruber, J Susskind, P Arkin (2003) The Version 2 Global Precipitation Climatology Project (GPCP) Monthly Precipitation Analysis (1979-Present). J Hydrometeor, **4,1147-1167.**

Akhil VP, F Durand, M Lengaigne, J Vialard, MG Keerthi, VV Gopalakrishna, C Deltel, F Papa, C de Boyer Montégut (2014) Processes of surface salinity seasonal cycle in the Bay of Bengal. J Geophys Res Oceans 116:3926-3947. doi : 10.1002/2013JC009632.

Akhil VP, M Lengaigne, J Vialard, F Durand, MG Keerthi, AVS Chaitanya, F Papa, VV Gopalakrishna, C de Boyer Montegut (2016) A modeling study of processes controlling the Bay of Bengal sea surface salinity interannual variability. J Geophys Res Oceans, 121, doi:10.1002/2016JC011662.

Akhil VP, J Vialard, M Lengaigne, MG Keerthi, J Boutin, J-l Vergely, F Papa (2020) Bay of Bengal Sea Surface Salinity variability using 8-years of improved SMOS re-processing. Rem Sens Envir, 248, doi: 10.1016/j.rse.2020.111964.

Aparna SG, JP McCreary, D Shankar, PN Vinayachandran (2012) Signatures of Indian Ocean Dipole and El Niño–Southern Oscillation events in sea level variations in the Bay of Bengal. J Geophys Res, 117, C10012, doi:10.1029/2012JC008055.

Behara A and PN Vinayachandran (2016) An OGCM study of the impact of rain and river water forcing on the Bay of Bengal. J Geophys Res Oceans, 121, 2425–2446, doi:10.1002/ 2015JC011325.

Benshila R, F Durand, S Masson, R Bourdalle-Badie, C de Boyer Montégut, F Papa, G Madec (2014) The upper Bay of Bengal salinity structure in a high-resolution model. Ocean Modelling, 74, 36-52, 2014.

Boutin J, Vergely J-L, Marchand S, D'Amico F, Hasson A, Kolodziejczyk Nicolas, Reul Nicolas, Reverdin G, Vialard J (2018) New SMOS Sea Surface Salinity with reduced systematic errors and improved variability. Remote Sensing Of Environment, 214, 115-134. Publisher's official version : https://doi.org/10.1016/j.rse.2018.05.022

Chaitanya AVS, M Lengaigne, J Vialard, VV Gopalakrishna, F Durand, C KranthiKumar, S Amrithash, V Suneel, F Papa, M Ravichandran (2014) Fishermen-operated salinity measurements reveal a "river in the sea" flowing along the east coast of India. BAMS, online

first, doi:http://dx.doi.org/10.1175/BAMS-D-12-00243.1

Chelton, D. B., DeSzoeke, R. A., Schlax, M. G., El Naggar, K., & Siwertz, N. (1998). Geographical variability of the first baroclinic Rossby radius of deformation. *Journal of Physical Oceanography*, *28*(3), 433-460.

Chelton DB, Schlax MG, Samelson RM (2011) Global observations of non-linear mesoscale eddies. Prog Oceanogr, doi:10.1016/ j.pocean.2011.01.002

Chen G, Li Y, Xie Q, Wang D (2018) Origins of eddy kinetic energy in the Bay of Bengal. Journal of Geophysical Research Oceans, 123, 2097–2115. https://doi.org/10.1002/2017JC013455.

Cotté C, F d'Ovidio, A Chaigneau, M Lèvy, I Taupier-Letage, B Mate, C Guinet (2011) Scale-dependent interactions of Mediterranean whales with marine dynamics, Limnology and Oceanography, *56*(1), 219–232, doi:10.4319/lo.2011.56.1.0219.

Dai A and KE Trenberth (2002) Estimates of freshwater discharge from continents: Latitudinal and seasonal variations, J Hydrometeorol, 3(6), 660–687

de Boyer Montégut C, G Madec, AS Fischer, A Lazar, D Iudicone (2004) Mixed layer depth over the global ocean: An examination of profile data and a profile-based climatology, J Geophys Res, 109, C12003, doi:10.1029/2004JC002378.

de Boyer Montégut C, J Mignot, A Lazard, S Cravatt (2007) Control of salinity on the mixed layer depth in the world ocean, Part I: General description. J Geophys Res, 112, C06011, doi:10.1029/2006JC003953.

Decharme B, Delire C, Minvielle M, Colin J, Vergnes J- P, Alias A, et al. (2019) Recent changes in the ISBA- CTRIP land surface system for use in the CNRM- CM6 climate model and in global off- line hydrological applications. Journal of Advances in Modeling Earth Systems, 11. https://doi. org/10.1029/2018MS001545

d'Ovidio F, Isern-Fontanet J, López C, Hernández-García E, García-Ladona E. (2009) Comparison between Eulerian diagnostics and finite-size Lyapunov exponents computed from altimetry in the Algerian basin. Deep-Sea Res, Pt. I, 56, 15–31, 2009. 786, 788.

Dibarboure D, et al, (2011) Jason-2 in DUACS: Up- dated system description, first tandem results and impact on processing and products. Mar Geod, 34, (3–4), 214–241.

Durand F, SR Shetye, J Vialard, D Shankar, SSC Shenoi, C Ethe, G Madec (2004) Impact of temperature inversions on SST evolution in the South-Eastern Arabian Sea during the pre-summer monsoon season. Geophys Res Lett, 31 (1) , L01305, 10.1029/2003GL018906.

Durand F, Shankar D, de Boyer Montégut C, Shenoi SSC, Blanke B, Madec G (2007) Modeling the barrier-layer formation in the southeastern Arabian Sea. Journal of Climate, 20(10), 2109-2120.

Durand F, D Shankar, F Birol, SSC Shenoi (2009) Spatiotemporal structure of the East India Coastal Current from satellite altimetry. J Geophys Res, 114, C02013, doi:10.1029/2008JC004807.

Fekete Balázs M, Vörösmarty Charles J, Grabs Wolfgang (2002) High-resolution fields of global runoff combining observed river discharge and simulated water balances. Global Biogeochemical cycles, Vol. 16, No. 3, 1042, doi :10.1029/1999GB001254, 2002.

Fournier S, Vialard J, Lengaigne M, Lee T, Gierach MM, Chaitanya AVS (2017a) Modulation of the Ganges- Brahmaputra river plume by the Indian Ocean dipole and eddies inferred from satellite observations. Journal of Geophysical Research Oceans, 122, 9591–9604. https://doi.org/10.1002/ 2017JC013333.

Fournier S, Vandemark D, Gaultier L, Lee T, Jonsson B, Gierach MM (2017b) Interannual variation in offshore advection of Amazon-Orinoco plume waters: Observations, forcing mechanisms, and impacts. Journal of Geophysical Research: Oceans, 122. https://doi.org/10.1002/2017JC013103.

Gopalakrishna VV, et al. (2002) "Upper ocean stratification and circulation in the northern Bay of Bengal during southwest monsoon of 1991." Continental Shelf Research 22.5 (2002): 791-802.

Gordon AL, EL Shroyer, A Mahadevan, D Sengupta, M Freilich (2016) Bay of Bengal: 2013 northeast monsoon upper-ocean circulation. *Oceanography* 29(2):82–91, http://dx.doi.org/10.5670/oceanog.2016.41.

Han W, JP McCreary, KE Kohler (2001) Influence of precipitation minus evaporation and Bay of Bengal rivers on dynamics, thermodynamics, and mixed layer physics in the upper Indian Ocean. J Geophys Res, 106, 6895–6916.

Hareeshkumar PV, B Matthew, MR Ramesh Kumar, AR Rao, PSV Jagadesh, KG Radhakrishnan, TN Shyni (2013) 'Thermohaline front' off the east coast of India and its generating mechanism. *Ocean Dyn*, **63,** 1175–1180, doi:10.1007/s10236 -013-0652-y.

Hormann V, Centurioni LR, Gordon AL (2019) Freshwater export pathways from the Bay of Bengal. Deep Sea Research Part II: Topical Studies in Oceanography, 104645.

Huffman GJ, et al. (2007) The TRMM Multisatellite Precipitation Analysis: Quasi-global, multiyear, combined-sensor precipitation estimates at fine scales. *J Hydrometeor*, **8,** 38 – 55, doi:10.1175 /JHM560.1.

Jensen TG (2001) Arabian Sea and Bay of Bengal exchange of salt and tracers in an ocean model. Geophys Res Lett, 28, 3967– 3970.

Krishnamohan KS, J Vialard, M Lengaigne, S Masson, G Samson, S Pous, S Neetu, F Durand, S Shenoi, G Madec (2019) Is there an effect of Bay of Bengal salinity on the Northern Indian Ocean Climatatological rainfall?, Deep Sea Research Part II: Topical Studies in Oceanography, Volume 166, 2019, Pages 19-33, ISSN 0967-0645, https://doi.org/10.1016/j.dsr2.2019.04.003.

Lumpkin R, Centurioni L, Perez RC (2016) Fulfilling observing system implementation requirements with the global drifter array. *Journal of Atmospheric and Oceanic Technology*, *33*, 685–695. https://doi.org/10.1175/JTECH-D-15-0255.1

Lehahn Yoav, d'Ovidio F, Koren Ilan (2018) A Satellite-Based Lagrangian View on Phytoplankton Dynamics. Annu Rev Mar Sci. 10:99-11, https://doi.org/10.1146/annurev-marine- 121916- 063204

Mahadevan A, G Spiro Jaeger, M Freilich, M Omand, EL Shroyer, D Sengupta (2016) Freshwater in the Bay of Bengal: Its fate and role in air-sea heat exchange. *Oceanography* 29(2):72–81, http://dx.doi.org/10.5670/oceanog.2016.40.

Masson S, J-J Luo, G Madec, J Vialard, F Durand, S Gualdi, E Guilyardi, S Behera, P Delecluse, A Navarra, T Yamagata (2005) Impact of barrier layer on winter-spring variability of the South-Eastern Arabian Sea, Geophys Res Lett, 32, L07703 10.1029/2004GL021980

McCreary JP, W Han, D Shankar, SR Shetye (1996) Dynamics of the East India Coastal Current: 2. Numerical solutions. J Geophys Res, 101, 13,993–14,010, doi:10.1029/96JC00560.

Morrow, R., Fu, L. L., D'Ovidio, F., & Farrar, J. T. (2019). Scientists invited to collaborate in satellite mission's debut. Eos, Trans. Amer. Geophys. Union, 100.

Neetu S, M Lengaigne, EM Vincent, J Vialard, G Madec, G Samson, MR Ramesh Kumar, F Durand (2012) Influence of upper-ocean stratification on tropical cyclone induced surface cooling in the Bay of Bengal. J Geophys Res, 117, C12020, doi:10.1029/2012JC008433.

Neetu S, M Lengaigne, J Vialard, G Samson, S Masson, KS Krishnamohan, I Suresh (2019) Premonsoon/Postmonsoon Bay of Bengal Tropical Cyclones Intensity: Role of Air- Sea

Coupling and Large- Scale Background State. Geophys Res Lett, 45, 2149-2157.

Papa F, SK Bala, RK Pandey, F Durand, VV Gopalakrishna, A Rahman, WB Rossow (2012) Ganga–Brahmaputra river discharge from Jason-2 radar altimetry: An update to the long-term satellite-derived estimates of continental freshwater forcing flux into the Bay of Bengal. J Geophys Res, 117, C11021, doi:10.1029/2012JC008158.

Pant V, MS Girishkumar, TVS Udaya Bhaskar, M Ravichandran, F Papa, VP Thangaprakash (2015) Observed interannual variability of near-surface salinity in the Bay of Bengal. *J Geophys Res Oceans*, 120, 3315–3329, doi:10.1002/2014JC010340.

Prasanna Kumar S, PM Muraleedharan, TG Prasad, M Gauns, N Ramaiah, SN de Souza, S Sardesai, M Madhupratap (2002) Why is the Bay of Bengal less productive during summer monsoon compared to the Arabian Sea?. Geophys Res Lett, 29(24), 2235, doi:10.1029/2002GL016013, 2002.

Praveen Kumar B, J Vialard, M Lengaigne, VSN Murty, MJ McPhaden (2012) TropFlux: Air-sea fluxes for the global tropical oceans-description and evaluation against observations. Clim Dyn, 38, 1521–1543.

Raj RP (2017) Surface velocity estimates of the North Indian Ocean from satellite gravity and altimeter missions. International Journal of Remote Sensing, 38(1), 296-313.

Rao RR, and R Sivakumar (2003) Seasonal variability of sea surface salinity and salt budget of the mixed layer of the north Indian Ocean. J Geophys Res, 108(C1), 3009, doi:10.1029/2001JC00907.

Rao SA, SK Behera, Y Masumoto, T Yamagata (2002) Interannual subsurface variability in the tropical Indian Ocean with a special emphasis on the Indian Ocean Dipole. Deep Sea Res, Part II, 49(7–8), 1549–1572, doi:10.1016/S0967-0645(01)00158-8.

Rao SA, Saha SK, Pokhrel S, Sundar D, Dhakate AR, Mahapatra S, et al. (2011) Modulation of SST, SSS over northern Bay of Bengal on ISO time scale. Journal of Geophysical Research, 116, C09026. https://doi.org/10.1029/2010JC006804

Saji NH, BN Goswami, PN Vinayachandran, T Yamagata (1999) A dipole mode in the tropical Indian Ocean, Nature, 401(6751), 360–363.

Sandeep KK, Pant V, Girishkumar MS, Rao AD (2018) Impact of riverine freshwater forcing on the sea surface salinity simulations in the Indian Ocean. J Mar Syst, 185, 40–58. https://doi.org/10.1016/j.jmarsys.2018.05.002

Sandeep KK and Pant V (2019) Riverine freshwater plume variability in the Bay of Bengal using wind sensitivity experiments. Deep Sea Research Part II: Topical Studies in Oceanography, 168, 104649.

Sarma VVSS, Rao GD, Viswanadham R, Sherin CK, Salisbury J, Omand MM, et al. (2016) Effects of freshwater stratification on nutrients, dissolved oxygen, and phytoplankton in the Bay of Bengal. Oceanography, 29(2), 222-231.

Schott FA and McCreary JP (2001) The monsoon circulation of the Indian Ocean. Progress in Oceanography, 51(1), 1–123.

Sengupta D, GN Bharath Raj, SSC Shenoi (2006) Surface freshwater from Bay of Bengal runoff and Indonesian throughflow in the tropical Indian Ocean. Geophys Res Lett, 33, L22609, doi:10.1029/2006GL027573.

Sengupta D, RG Bharath, DS Anitha (2008) Cyclone-induced mixing does not cool SST in the post-monsoon north Bay of Bengal. Atmos Sci Lett, 9, 1–6, doi:10.1002/asl.162.

Sengupta D, GN Bharath Raj, M Ravichandran, J Sree Lekha, F Papa (2016) Near-surface salinity and stratification in the north Bay of Bengal from moored observations, Geophys Res Lett, 43, 4448–4456, doi:10.1002/2016GL068339.

Shankar D, JP McCreary, W Han, SR Shetye (1996) Dynamics of the East India Coastal Current 1. Analytic solutions forced by interior Ekman pumping and local alongshore winds. J Geophys Res, 101, 13,975–13,991, doi:10.1029/96JC00559.

Shankar D, Vinayachandran PN, Unnikrishnan AS (2002) The monsoon currents in the north Indian Ocean. Progress in oceanography, 52(1), 63-120.

Sherin VR, Durand F, Gopalkrishna VV, Anuvinda S, Chaitanya AVS, Bourdallé-Badie R, Papa F (2018) Signature of Indian Ocean Dipole on the western boundary current of the Bay of Bengal. Deep Sea Research Part I: Oceanographic Research Papers, 136, 91-106.

Shetye SR, Shenoi SSC, Gouveia AD, Michael GS, Sundar D, Nampoothiri G (1991) "Wind-driven coastal upwelling along the western boundary of the Bay of Bengal during the southwest monsoon". Continental Shelf Research 11.11 (1991): 1397-1408.

Shetye SR, AD Gouveia, D Shankar, SSC Shenoi, PN Vinayachandran, D Sundar, GS Michael, G Nampoothiri (1996) Hydrography and circulation in the western Bay of Bengal during the northeast monsoon. J Geophys Res, 101(C6), 14,011–14,026.

Sree Lekha J, Buckley JM, Tandon A, Sengupta D (2018) Subseasonal dispersal of freshwater in

the northern Bay of Bengal in the 2013 summer monsoon season. *Journal of Geophysical Research: Oceans, 123*. https://doi.org/ 10.1029/2018JC014181

Sudre Joel, Maes Christophe and Veronique Garcon (2013) On the global estimates of geostrophic and Ekman surface currents. Limnology and Oceanography: Fluids and Environments 3 (2013): 1–20 DOI 10.1215/21573689-2071927

Suresh I, Vialard J, Lengaigne M, Izumo T, Parvathi V, Muraleedharan PM (2018) Sea level interannual variability along the west coast of India. Geophysical Research Letters, 45, 12,440–12,448. https://doi.org/10.1029/ 2018GL080972.

Thadathil P, I Suresh, S Gautham, S Prasanna Kumar, M Lengaigne, RR Rao, S Neetu, and A Hegde (2016) Surface layer temperature inversion in the Bay of Bengal: Main characteristics and related mechanisms. J Geophys Res Oceans, 121, 5682–5696, doi:10.1002/ 2016JC011674.

Vinayachandran PN, VSN Murty, V Ramesh Babu (2002) Observations of barrier layer formation in the Bay of Bengal during summer monsoon, J Geophys Res, 107(C12), 8018, doi:10.1029/2001JC000831.

Vinayachandran PN, Shankar D, Kurian J, Durand F, Shenoi SSC (2007) Arabian Sea mini warm pool and the monsoon onset vortex. Current Science, 203-214.

Vinayachandran PN, D Shankar, S Vernekar, KK Sandeep, P Amol, CP Neema, and A Chatterjee (2013) A summer monsoon pump to keep the Bay of Bengal salty. Geophysical Research Letters, 40 (9), pp. 1777-1782.

Webster PJ, AM Moore, JP Loschnigg, and RR Leben (1999) Coupled ocean-atmosphere dynamics in the Indian Ocean during 1997 - 98. Nature, 401(6751), 356–60, doi:10.1038/43848.

Wijesekera HW, Shroyer E, Tandon A, Ravichandran M, Sengupta D, Jinadasa SUP, et al. (2016) ASIRI: An Ocean–Atmosphere Initiative for Bay of Bengal. Bulletin of the American Meteorological Society, 97(10), 1859–1884. doi:10.1175/bams-d-14-00197.1

Wilson EA and Riser SC (2016) An assessment of the seasonal salinity budget for the upper Bay of Bengal. Journal of Physical Oceanography, 46(5), 1361-1376.

Mis en forme

	Total (km^3)	P-E (%)	GB (%)	IRS (%)	MGKNE (%)	Other rivers (%)
Fekete et al. (2002) & TRMM	5797	52	22	15	5	6
Fekete et al. (2002) & GPCP	5145	45	25	16	6	8

Table 1. Climatological contributions of various freshwater sources to the total Bay of Bengal local freshwater input over the 15th May to 15th December period, during which the BoB gains most of its freshwater (Figure 1c).

Experiments	***Currents***
CTL	*Full GECKO currents*
NOED	*No eddies (seasonal cycle + large scale interannual anomalies, see section 2.3)*
NOEK	*No Ekman drift (surface geostrophic component (AVISO))*

Table 2. Summary of the various Lagrangian experiments used in this study. All experiments are run for each year over the 2000-2016 period, starting on the 15th of Jun, Jul, Aug, Sep, Oct & Nov of each year and ending on February 15th of the following year. Results presented in the paper correspond to 2000-2016 averages, generally shown for October and December 15th. Section 4.1 details how the results of the Lagrangian computations are combined with river runoff and precipitation minus evaporation observational estimates to yield maps of the freshwater distribution over the August to February period for each year. Each simulation accounts for freshwater inputs over the preceding month, i.e. we account for 15th May to 15th December freshwater inputs in our experiments (see shading on Figure 1c).

Figures

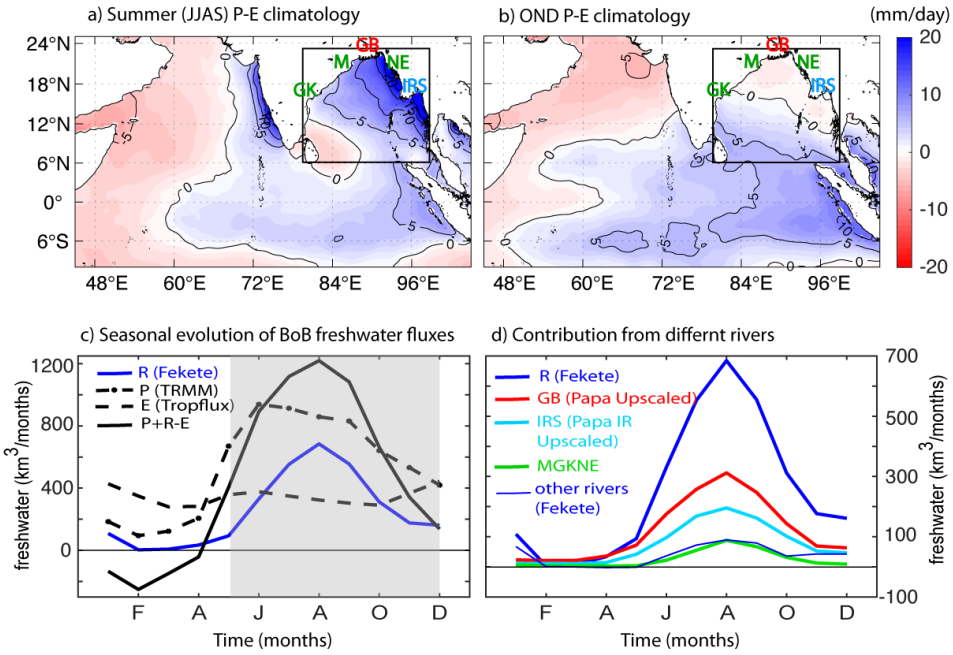

Figure 1. (a) Summer monsoon (June to September) and **(b)** winter monsoon (October to December) observed averaged climatological precipitation minus evaporation (TRMM for precipitation and Tropflux for evaporation, shading with contours every 5 mm day-1). The locations of the major river outlets in terms of Bay of Bengal (BoB) freshwater inputs are marked (GB for Ganges-Brahmaputra, IRS for Irrawaddy-Salween, M for Mahanadi, GK for Godavari-Krishna and NE for other rivers in the Northeast, notably the Kaladan river). **(c)** Monthly climatological freshwater flux ($km^3.month^{-1}$) into the BoB (defined as the black frame on panels a and b) from rivers (R, blue), rain (P, dot-dashed black), evaporation (E, dashed black) and P+R-E (continuous black). The grey shading highlights the period during which freshwater inputs are tracked using a Lagrangian method in this work. **(d)** Monthly climatological river freshwater flux from all rivers into BoB (R, continuous line), the Ganges-Brahmaputra (GB, red), Irrawaddy-Salween (IRS, light blue), other rivers accounted for in this study (MGKNE, green) rivers, and the remaining BoB rivers (thin dark blue line). The river discharges are estimated from Fekete et al. (2002, blue) and Papa et al. (2012, red) for GB and IR, the rainfall from TRMM, and Evaporation from Tropflux (see section 2.1 for details).

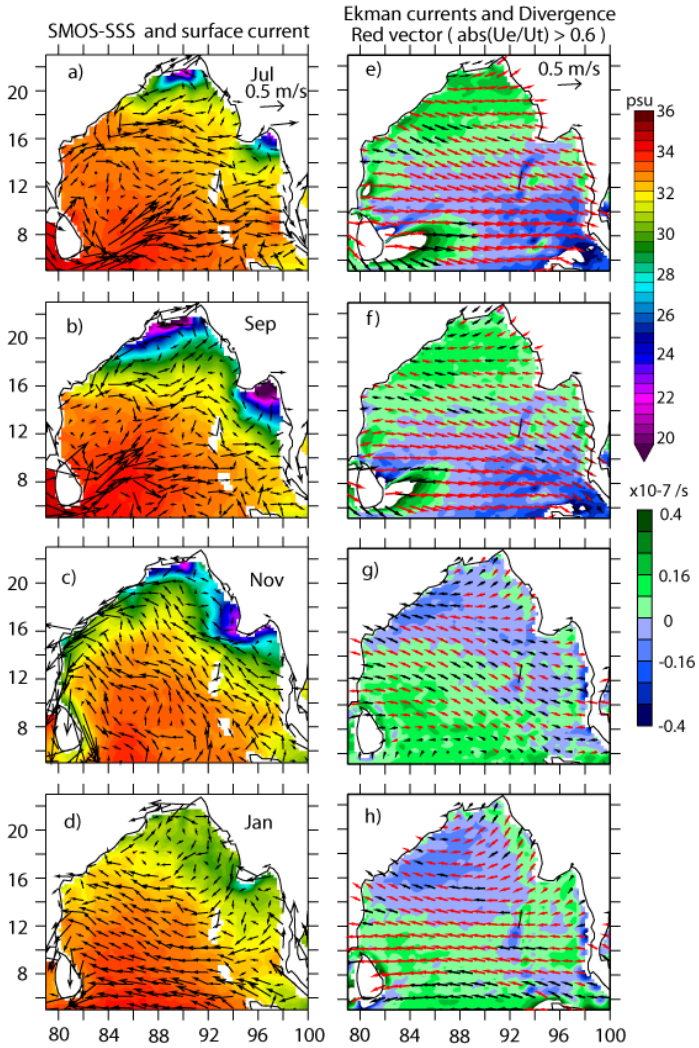

Figure 2. (Left panels) Monthly seasonal climatology of sea surface salinity (SSS, psu, shading) and total (geostrophic + Ekman) surface currents ($m.s^{-1}$, vectors) in the BoB for **(a)** July, **(b)** September, **(c)** November and **(d)** January. **(Right panels)** Monthly seasonal climatology of climatological Ekman currents (vectors, with red vectors indicating locations where Ekman currents accounts for more than 2/3 of the total surface zonal current) and their divergence (10^{-7} s^{-1}, shading). The climatological SSS is obtained from the SMOS satellite dataset (2010-2016 period) and the currents from the GECKO dataset (2000-2016 period, see section 2.1 for details).

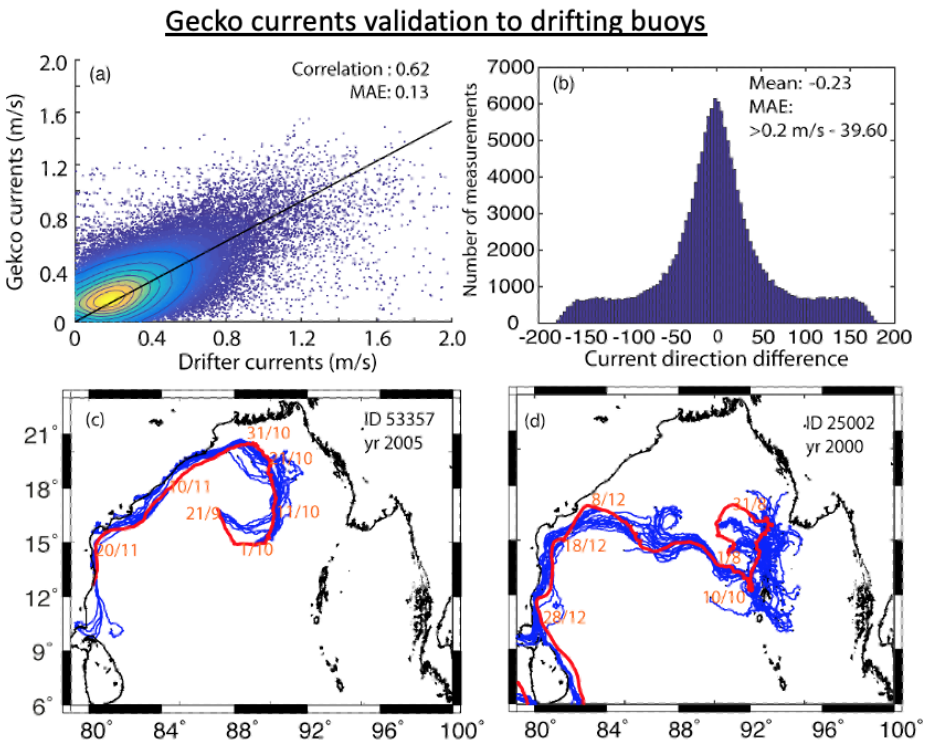

Figure 3. (a) Scatterplot of drifters against the collocated GECKO surface current velocity. The associated correlation and Mean Absolute Error (MAE) are indicated on the upper right. **(b)** Probability distribution of the angle difference between the drifter and collocated GECKO currents. The associated mean angle error, and MAE for drifter currents above 0.2 $m.s^{-1}$ are indicated on the upper right. **(c,d)** Trajectories from two selected drifters and from 30 days trajectories deducted from GECKO using a Lagrangian tool (see text for details). A trajectory is generated every 10 days along the observed drifter track, with a random walk process applied to the Lagrangian computation, in order to mimic Laplacian lateral mixing with a mixing coefficient of 300 m^2s^{-1} (see text for details).

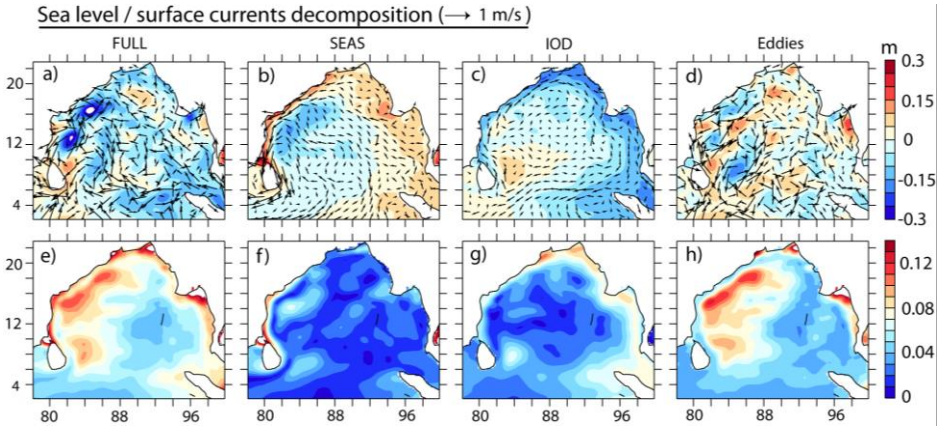

Figure 4. (a) Snapshot of sea level anomaly (SLA, m, shading) and surface currents ($m.s^{-1}$, vectors) on the 15th November 2006 (positive IOD year) and its decomposition into **(b)** the climatological seasonal cycle**, (c)** large-scale interannual anomalies (derived from an Empirical Orthogonal Function analysis, see section 2.3 for details) and **(d)** synoptic current anomalies (i.e. mainly eddies, derived as the residual). SLA standard deviation computed over the 2000-2016 period for **(e)** the full field, **(f)** the seasonal cycle, **(g)** large-scale and **(h)** eddies.

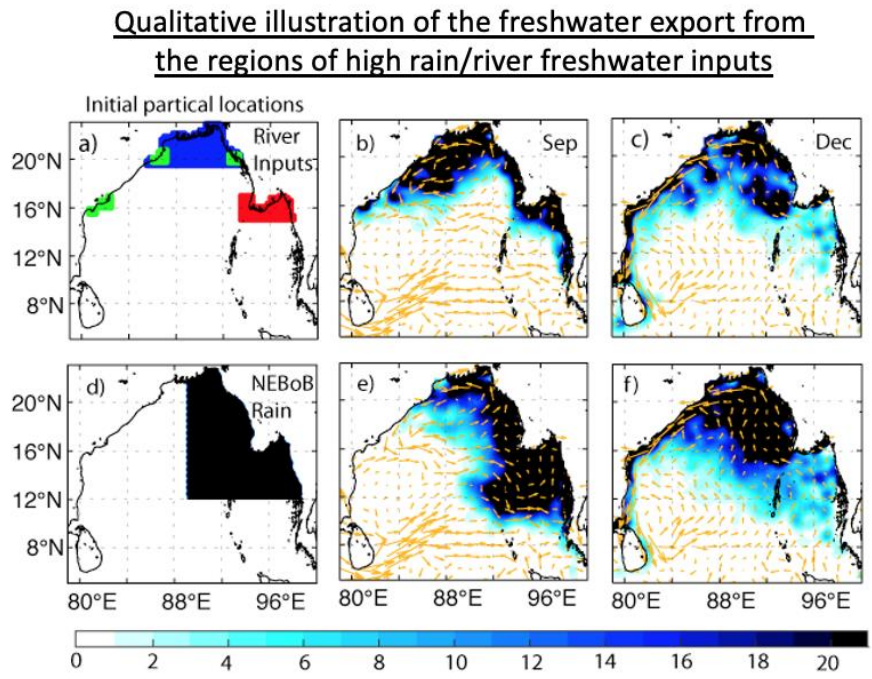

Figure 5. Average particles density (number of particles per 0.25° x 0.25^0 cell) for **(a)** particles released on August 15th with a uniform particle density near the major river outlets (GB in blue, IRS in red, MGKNE in green) and their distributions on **(b)** September 15th and **(c)** December 15th. **(d-f)** as (a-c) but for particles initially released in the northeastern BoB (NEBOB), the region of strongest climatological precipitation over the BoB (see Figure 1a). Particles are advected forward in time using GECKO currents starting for each year over the 2000-2016 period. The 2000-2016 average particles density are plotted. Average currents over the entire Lagrangian simulation (i.e. from August 15th to the date of each panel) are plotted as orange vectors on the two left columns. This figure *qualitatively* illustrates the effects of the circulation by showing the density of particles released near river mouths (panel a) and in the strongest rain region (panel d). The *quantitative* method to compute the Lagrangian freshwater distribution is discussed in section 4 with the support of the Figure 8 sketch.

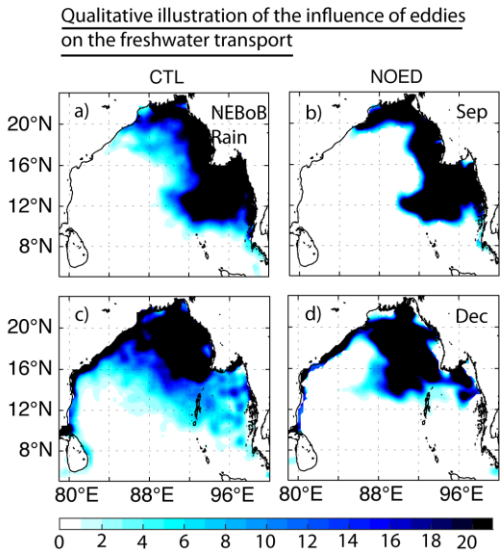

Figure 6: Average particle density maps (number of particles per 0.25° x 0.25° cell) on **(a,b)** September 15th and **(d,e)** December 15th for particles uniformly released in the northeastern BOB region (see Figure 5d for the initial distribution) on the 15th of August, computed using **(a, c)** full currents and **(b, d)** large-scale currents (i.e. no eddies, NOED). Particles are advected forward in time using GECKO currents for each year over the 2000-2016 period. The 2000-2016 average particles density are plotted. This figure *qualitatively* illustrates the effects of eddies on freshwater redistribution by showing the density evolution of particles released in the strongest rain region (panel d; experiments with particles initially released at the major river mouths show the same qualitative features). The *quantitative* method to compute the Lagrangian freshwater distribution is discussed in section 4 with the support of the Figure 8 sketch.

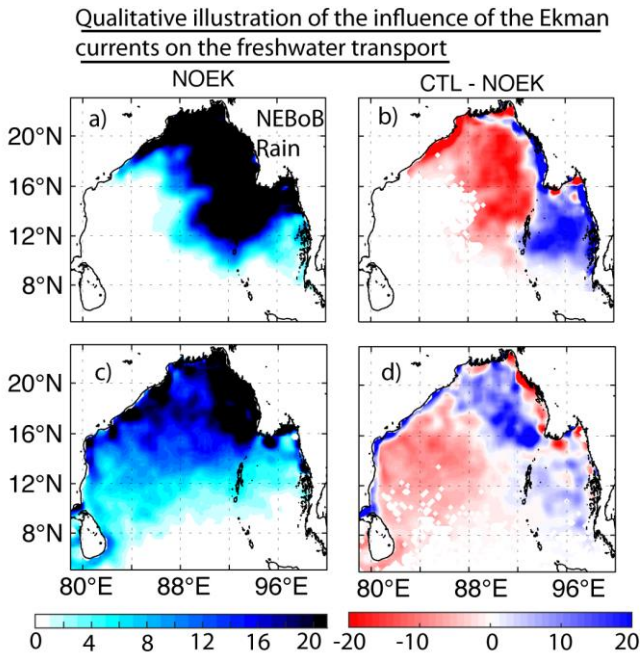

Figure 7: Average particle density maps (number of particles per 0.25° x 0.25° cell) on **(a,b)** September 15th and **(d,e)** December 15th for particles uniformly released in the northeastern BOB region (see Figure 5d for the initial distribution) on the 15th of August, computed using **(a, c)** geostrophic currents (i.e. no Ekman component, NOEK), **(b, d)** difference between particle density maps computed using full currents (see Figure 6ac) and geostrophic currents (CTL - NOEK). Particles are advected forward in time using GECKO currents for each year over the 2000-2016 period. The 2000-2016 average particles density are plotted. This figure *qualitatively* illustrates the effects of the Ekman currents on freshwater redistribution by showing the density evolution of particles released in the strongest rain region (panel d; experiments with particles initially released at the major river mouths show the same qualitative features). The *quantitative* method to compute the Lagrangian freshwater distribution is discussed in section 4 with the support of the Figure 8 sketch.

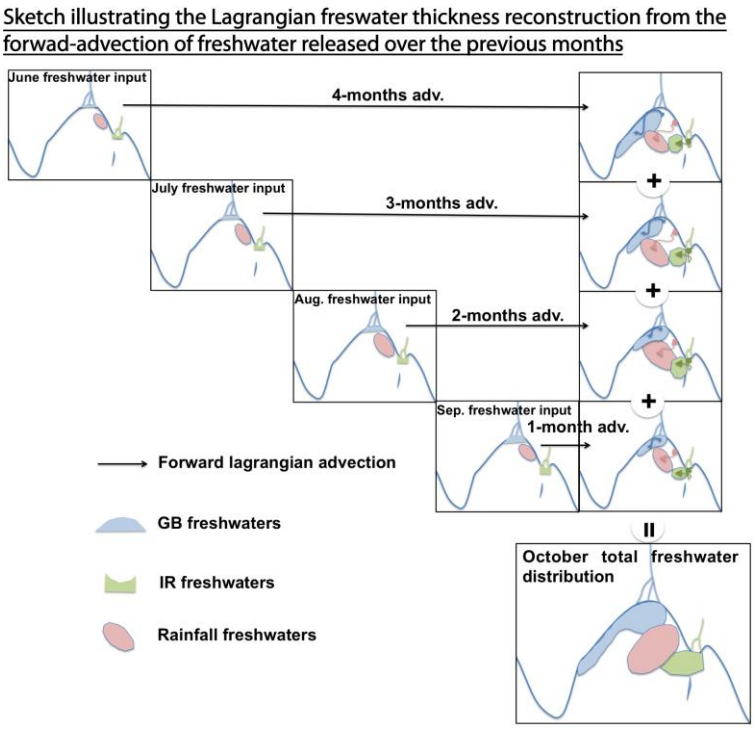

Figure 8. Sketch explaining how the Lagrangian freshwater thickness distribution from individual sources is reconstructed based on the forward-advection of freshwater released over the previous months, here for the example of October. Lagrangian computations initialized over the previous months are combined to provide quantitative estimates of the freshwater distributions associated with river inputs (GB in Blue; IRS in green; we also track freshwater from other smaller rivers indicated by letters on Figure 1a, but did not represent them on this sketch) and Precipitation minus Evaporation (P-E, red: the main source of rain freshwater in the Northeastern BoB is represented on this sketch, but P-E freshwater is in fact traced everywhere, including outside of the BoB). From June onwards, virtual drifters are launched every month. Every particle tracks the freshwater volume received over its 0.025° x 0.025° initial location during the month preceding its release, using as many variables as needed (e.g. a particle near the GB will track separately the freshwater it received from rain and from the GB; these separate freshwater distribution are represented using colors on the sketch). They are then advected forward using satellite estimates of the total surface currents until October. As they are advected they do not acquire, or lose, any further freshwater. Cumulating freshwater released in June, July, August and September within ¼° bins allows to get the freshwater distribution associated to each source in October.

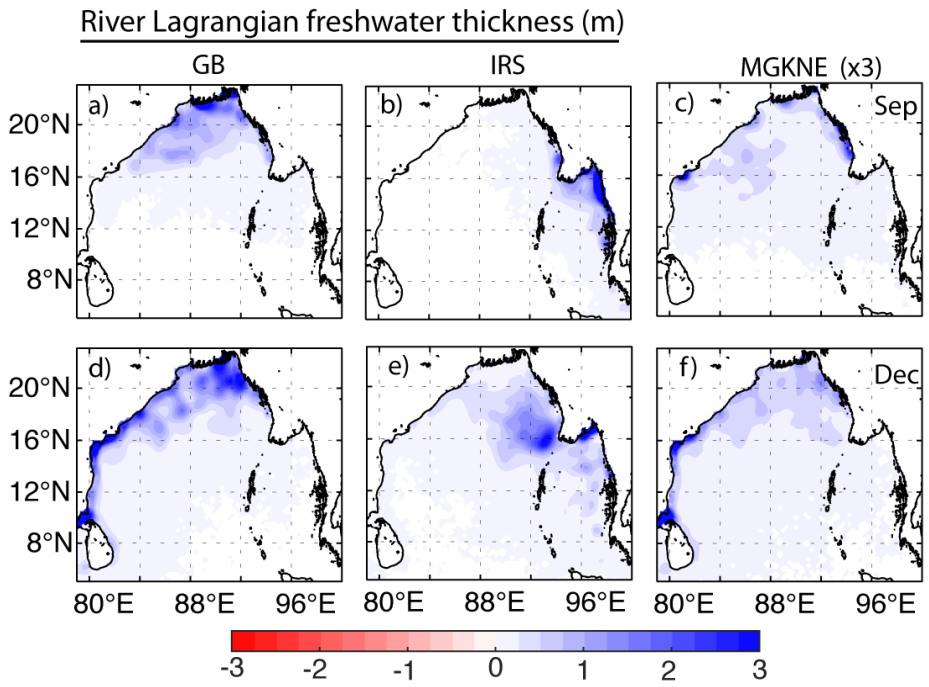

Figure 9. 2000-2016 average river Lagrangian freshwater thickness (m) maps on **(a,b,c)** September 15th and **(d,e,f)** December 15th for various rivers: **(a, d)** Ganges-Brahmaputra (GB), **(b,e)** Irrawady-Salween (IRS) and **(c,f)** Mahanadi, Godavari, Krishna, and other rivers in the Northeast (MGKNE, see Figure 1b for the river mouth locations). Note that the Lagrangian freshwater thickness associated with MGKNE river inputs has been multiplied by 3 for more readability. The Lagrangian freshwater distribution is obtained for each year over 2000-2016 using the procedure described from the sketch of Figure 8, and the 2000-2016 average is plotted.

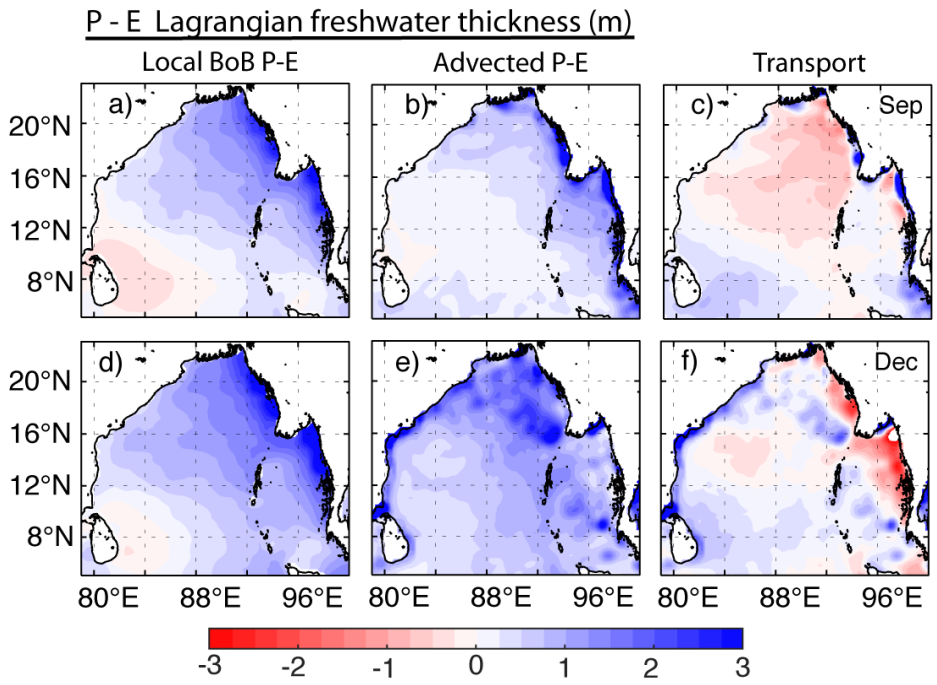

Figure 10. (a) June to September cumulated Precipitation minus Evaporation, **(b)** advected Precipitation minus evaporation using the Lagrangian method (procedure described on the sketch of Figure 8), **(c)** net effect of freshwater transport obtained as panel b minus panel a. **(d,e,f)** as (a,b,c) but for June to December cumulated freshwater input due to Precipitation minus Evaporation. The Lagrangian freshwater distribution is obtained for each year over 2000-2016, and the 2000-2016 average is plotted.

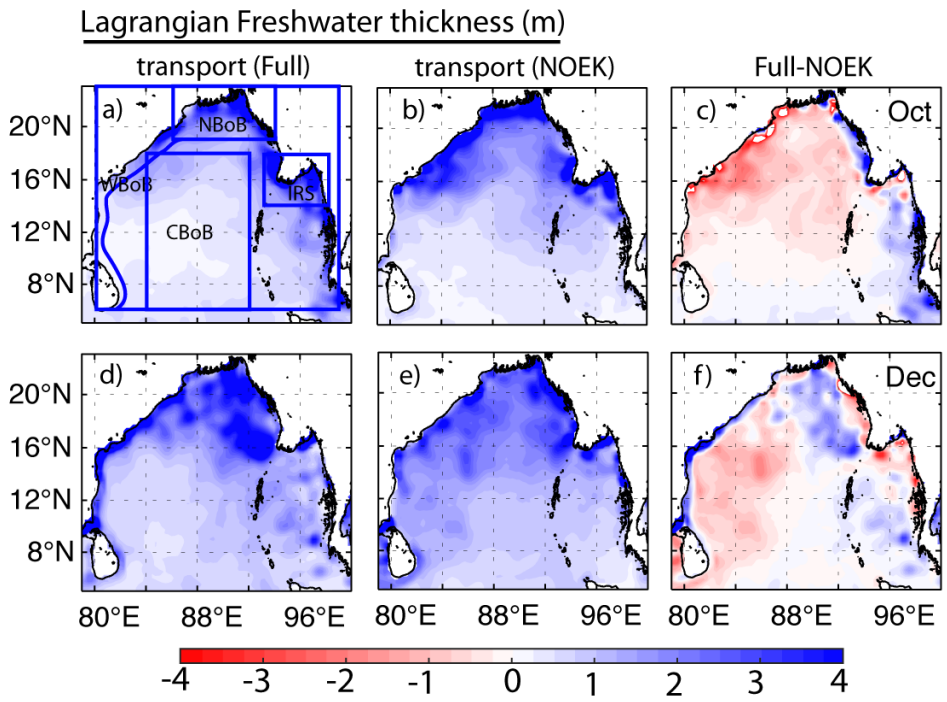

Figure 11. (a) 2000-2016 average total (i.e. P-E and rivers) Lagrangian freshwater thickness (m) map on September 15th. **(b)** As panel (a) but for the Lagrangian experiment that does not account for Ekman currents NOEK. **(c)** Panel (a) minus panel (b), which gives the net effect of Ekman current on the Lagrangian freshwater thickness distribution. **(d-f)** as (a,c) but for the December 15th freshwater distribution. The Lagrangian freshwater distribution is obtained for each year over 2000-2016 using the procedure described on the sketch of Figure 8, and the average is plotted. Blue boxes on panel (a) indicate regions used for budget computations in Figure 13, 14 & 15.

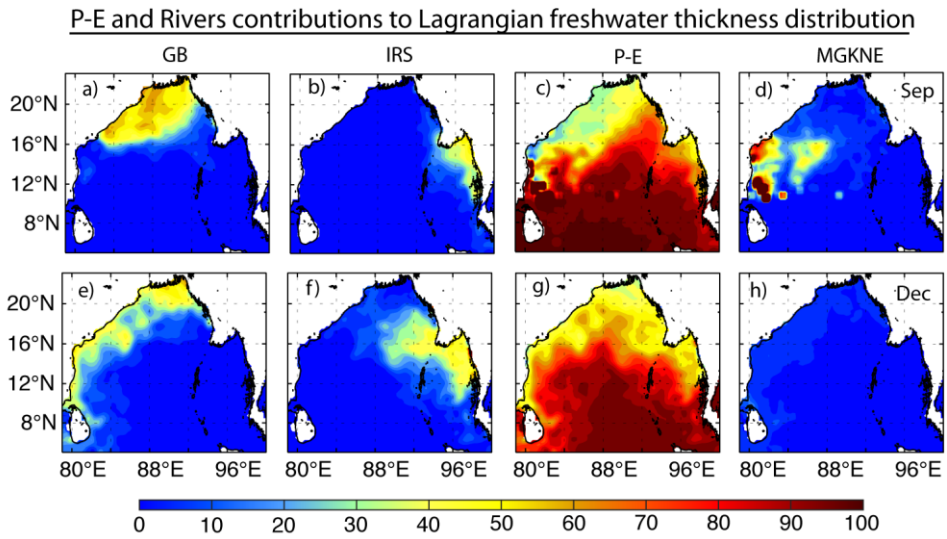

Figure 12: 2000-2016 average maps of contributions from individual sources to the total Lagrangian freshwater distribution (%) on September 15th, for **(a)** Ganges-Brahmaputra (GB), **(b)** Irrawaddy-Salween (IRS), **(c)** precipitation minus evaporation and **(d)** other rivers (MGKNE, see Figure 1a for river mouth locations). **(e-h)** same as (a-d) but for December 15th. See Figure 1b for the various river mouth locations.

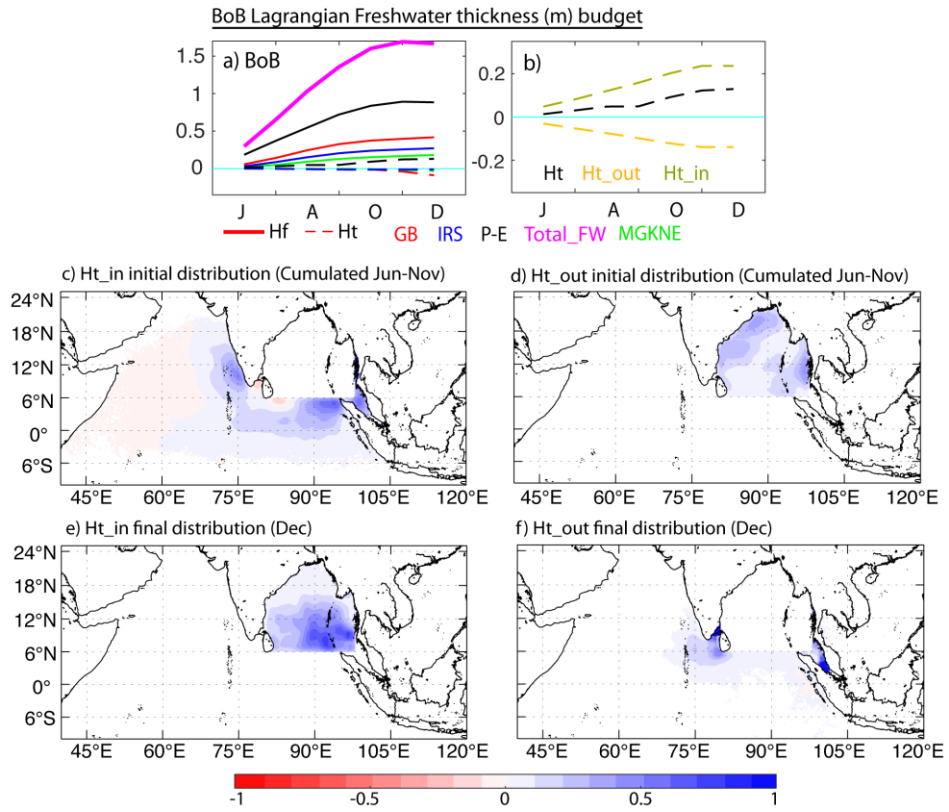

Figure 13. (a) 2000-2016 average Lagrangian freshwater thickness (m) budget for the BoB (see Figure 11a for the region definition). The average total Lagrangian freshwater thickness (magenta curve, m) is decomposed into local inputs into the box (plain lines) and net effect of transport (dashed lines) from the Ganges-Brahmaputra (GB, red curves), Irrawaddy-Salween (IRS, blue curves), and other rivers (MGKNE, green curve) and precipitation minus evaporation (P-E, black curves). **(b)** Net P-E freshwater transport into the BoB (dashed line on panel a, note the different y-axis scale) decomposed into what comes into the BoB ($H_{t\ in}$) and what comes out ($H_{t\ out}$). **(c, e)** Initial and final P-E Lagrangian freshwater thickness associated with inputs into the BoB $H_{t\ in}$. **(d, f)** Initial and final P-E Lagrangian freshwater thickness associated with inputs into the BoB $H_{t\ out}$.

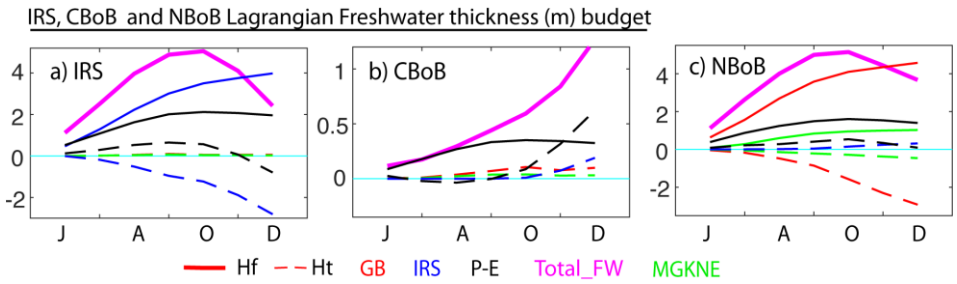

Figure 14. 2000-2016 average Lagrangian freshwater thickness (m) budgets for the IRS, NBoB and CBoB regions (see Figure 11a for region definition): **(a)** the Irrawaddy river mouth region, **(b)** the Central Bay of Bengal and **(c)** the Northern Bay of Bengal (encompassing the GB mouth). The average total Lagrangian freshwater thickness in each region (magenta curve, m) is decomposed into local inputs into the box (plain lines) and net effect of transport (dashed lines) from the Ganges-Brahmaputra (GB, red curves), Irrawaddy-Salween (IRS, blue curves), other rivers (MGKNE, green curve) and precipitation minus evaporation (P-E, black curves). Note the different y-axis ranges for each panel.

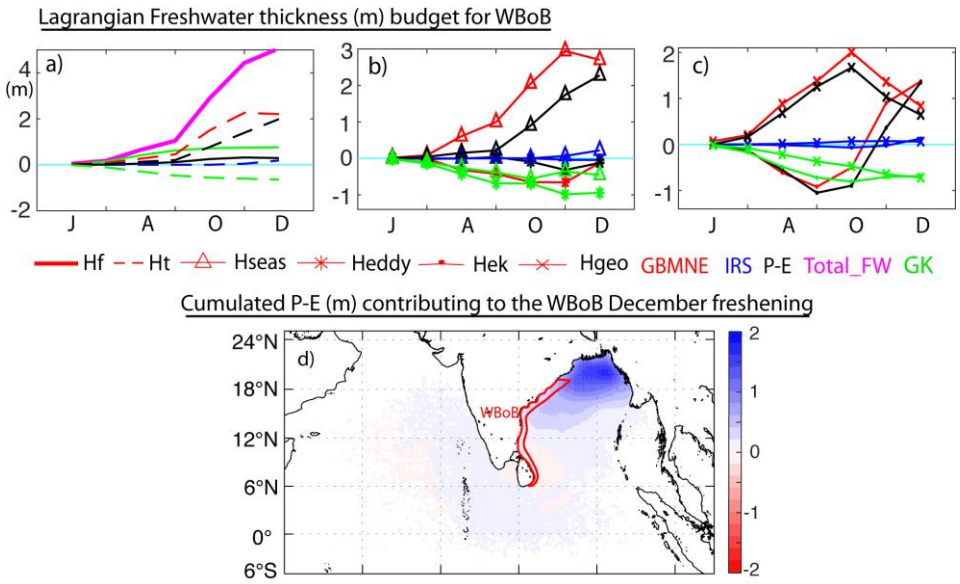

Figure 15. (a) 2000-2016 average Lagrangian freshwater thickness (m) budget for the WBOB region (see panel d for region definition). The average total Lagrangian freshwater thickness (magenta curve, m) is decomposed into local inputs into the box (plain lines) and net effect of transport (dashed lines) from rivers in the northern Bay (Ganges-Brahmaputra, Mahanadi, rivers in the Northeast: GBMNE, red curves), Irrawaddy-Salween (IRS, blue curves), Godavari and Krishna (GK, green curve) and precipitation minus evaporation (P-E, black curves). The net transport contributions of panel (a) are further decomposed into their **(b)** seasonal (triangles) and eddy (stars) contributions and **(c)** geostrophic (crosses) and Ekman (dots) currents contributions. **(d)** Cumulative June to November distribution of Precipitation minus Evaporation (P-E) contributing to the WBoB (red frame) December freshening. This can be seen as the "watershed" that contributes to the December input of precipitation minus evaporation into the WBOB region. Note the different y-axis ranges for panels (a) and (b,c).

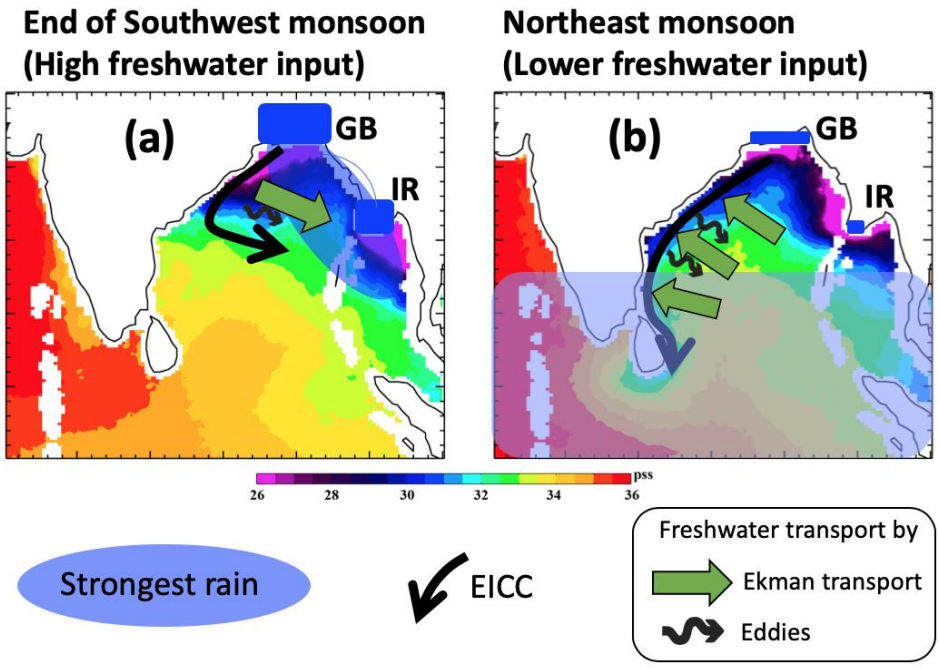

Figure 16. Schematic of the freshwater redistribution by the circulation **(a)** at the end of the southwest monsoon and **(b)** during the northeast monsoon**. (a)** During the Southwest monsoon, the rain, and rivers (GB: Ganges-Brahmaputra and IR: Irrawaddy) freshwater input is very strong, with most rain occurring in the northeastern BoB. The EICC is inefficient in exporting freshwater southward at the end of the southwest monsoon, because the rain and GB freshwater it captures is exported offshore by mesoscale eddies and the southwestward Ekman transport. The southwestward Ekman transport also pushes the Irrawaddy water toward the coast. (b) During the Northeast monsoon, the GB, IR and rain freshwater inputs are much lower, with most rain in the southwestern Bay of Bengal. The freshwater is however more efficiently exported southward by the coastally-trapped EICC, because the shoreward Ekman transport is stronger than the offshore export by meso-scale eddies, and maintains freshwater near the coast, in the EICC. The EICC freshwater route to the Bay of Bengal "exit" near Sri Lanka is hence most efficient during the low freshwater input period, explaining why relatively small fractions of the GB (~22%) and rain (~9 %) exit the BoB via this route.

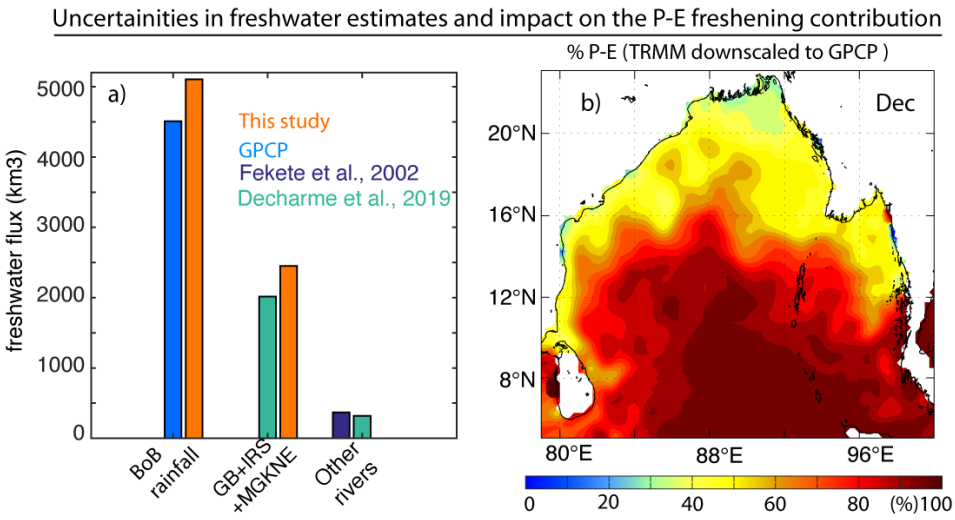

Figure 17. (a) June-December total climatological freshwater flux into the BoB (north of 6°N) estimated from different datasets: this study (based on TRMM date, see methods section for details) and GPCP for rainfall; this study (based on Fekete et al. (2002) data, see methods section for details) and Decharme et al. (2019) for the Bay of Bengal largest rivers (GB+IRS+MGKNE, i.e. Ganges-Brahmaputra, Irrawaddy-Salween; Godavari-Krishna and other rivers in the northeastern Bay; see Figure 1a for location). **(b)** Percentage of freshwater originating from P-E of the 15th December as in Figure 12g but when using GPCP rainfall instead of TRMM.